

Carbon Stocks and Potential Greenhouse Gas Release of Permafrost-affected Active Floodplains in the Lena River Delta

Master Thesis

for attainment of the academic degree of
Master of Science
in the study program Environmental Sciences

presented by

Tanja Herbst

4922056

Frist Supervisor: Prof. Dr. Guido Grosse

Second Supervisor: Prof. Dr. Christiane Werner



Faculty of Environment and Natural Resources

Albert-Ludwigs-University

Freiburg im Breisgau 2022

Abstract

Arctic warming increases the degradation of permafrost soils. This makes large deposits of formerly frozen organic matter vulnerable to microbial decomposition, resulting in the release of methane (CH₄) and carbon dioxide (CO₂) to the atmosphere. The active floodplains in Arctic river deltas are highly dynamic permafrost environments due to active erosion and sedimentation but they are so far understudied. Therefore, this study aims to determine soil organic carbon (SOC) and soil nitrogen (SN) stocks, accumulation rates, and the potential CH₄ and CO₂ release from the active floodplains of Kurungnakh and Samoylov Island in the Lena River Delta. Key soil properties were analyzed and a 68-day incubation at 20 °C under aerobic and anaerobic conditions was performed. The mean SOC and SN stocks were 12.89 ± 6.02 kg C m⁻² and 0.56 ± 0.38 kg N m⁻², respectively, with ~40% stored in the upper 30 cm. The stocks showed a high heterogeneity in terms of depth-distribution. The estimated SOC pool for the active floodplains in the entire Lena River Delta was $\sim 114 \pm 53$ Tg C. Total anaerobic CH₄ emissions ranged from 0.03 ± 0.01 to 176.95 ± 13.35 μg CH₄-C gsoil⁻¹. The active layer samples did not reach a steady state during incubation period, and the permafrost layer samples showed a 30-day lag phase. CO₂ emissions (9.14 ± 1.31 to 417.33 ± 31.39 μg CO₂-C gsoil⁻¹ anaerobically and 17.47 ± 1.57 to 856.12 ± 61.37 μg CO₂-C gsoil⁻¹ aerobically) were mostly two times higher under aerobic conditions than under anaerobic conditions, but both treatments showed a similar pattern during incubation. Correlations were found between emissions (per gram of dry soil) and total organic carbon, and soil texture. The comparison of emissions per gram of dry soil and per gram of soil carbon indicated that not only carbon quantity but also its quality had an important impact on decomposition. This comprehensive study provides valuable information on the carbon stocks and carbon release from active floodplains in the Lena River Delta and highlights the need to include these dynamic permafrost environments in future estimates of the permafrost carbon climate feedback.

Zusammenfassung

Die Erwärmung der Arktis verursacht ein zunehmendes Tauen der Permafrostböden. Hierdurch werden große Mengen an zuvor gefrorenem organischem Material für mikrobielle Zersetzung verfügbar, was zur Freisetzung von Methan (CH₄) und Kohlendioxid (CO₂) führt. Die aktiven Überschwemmungsgebiete in arktischen Flussdeltas sind aufgrund regelmäßiger Erosions- und Sedimentationsprozesse sehr dynamische Permafrostlandschaften, die bislang wenig untersucht wurden. Ziel dieser Studie ist daher, die Menge an organischem Kohlenstoff und Stickstoff im Boden, die Kohlenstoff- und Sedimentakkumulation sowie die potenzielle Freisetzung von CH₄ und CO₂ in den aktiven Überschwemmungsgebieten des sibirischen Lena Deltas zu untersuchen. Hierfür wurden verschiedene Bodeneigenschaften analysiert und eine 68-tägige Inkubation bei 20 °C unter aeroben und anaeroben Bedingungen durchgeführt. Die durchschnittlichen Kohlenstoff- und Stickstoffspeicher lagen bei $12.89 \pm 6.02 \text{ kg C m}^{-2}$ bzw. $0.56 \pm 0.38 \text{ kg N m}^{-2}$, wovon ~40 % in den oberen 30 Zentimetern gespeichert waren. Die Kohlenstoffgehalte variierten stark mit der Tiefe. Der gesamte Kohlenstoffspeicher der aktiven Überschwemmungsgebiete im Lena Delta beträgt $\sim 114 \pm 53 \text{ Tg C}$. Die kumulativen CH₄-Emissionen unter anaeroben Bedingungen lagen zwischen 0.03 ± 0.01 und $176.95 \pm 13.35 \text{ } \mu\text{g CH}_4\text{-C gBoden}^{-1}$. Die Emissionen der Bodenproben der jährlichen Auftauschicht schwankten über den Inkubationszeitraum und die Bodenproben der Permafrostschicht zeigten bis Tag 30 keine CH₄-Produktion. Die CO₂-Emissionen (anaerob: 9.14 ± 1.31 bis $417.33 \pm 31.39 \text{ } \mu\text{g CO}_2\text{-C gBoden}^{-1}$; aerob: 17.47 ± 1.57 bis $856.12 \pm 61.37 \text{ } \mu\text{g CO}_2\text{-C gBoden}^{-1}$) waren unter aeroben Bedingungen meist doppelt so hoch wie unter anaeroben Bedingungen, jedoch zeigten die beiden Raten ein ähnliches Muster während der Inkubation. Aus den geochemischen Untersuchungen und den Emissionsraten ließen sich Zusammenhänge zwischen den Emissionen und dem Kohlenstoffgehalt sowie der Bodentextur ermitteln. Der Vergleich der Emissionen pro Gramm Trockenbodengewicht und pro Gramm Bodenkohlenstoff zeigte die Bedeutung der Kohlenstoffqualität bei der Zersetzung von organischem Material. Diese Studie liefert wichtige Informationen zu den sehr dynamischen und heterogenen aktiven Überschwemmungsgebieten in Flussdeltas und hilft Schätzungen von Klimamodellen zu tauenden Permafrostböden verbessern.

Table of Contents

List of Figures.....	VII
List of Tables.....	VIII
Abbreviations	IX
1 Introduction	1
2 Materials and Methods	4
2.1 Study Area	4
2.2 Site Description, Soil Coring and Sampling.....	6
2.3 Soil Characteristics	7
2.3.1 pH Value and Electric Conductivity.....	7
2.3.2 Water Content.....	9
2.3.3 Grain Size	9
2.3.4 Carbon and Nitrogen Analysis	10
2.3.5 Organic Carbon and Total Nitrogen Stocks	10
2.3.6 Carbon and Nitrogen Pools of Active Floodplains.....	10
2.3.7 Radiocarbon Dating.....	11
2.3.8 Carbon and Sediment Accumulation Rates	11
2.4 Incubation Experiment.....	12
2.4.1 Description of Incubated Samples.....	12
2.4.2 Incubation Setup	13
2.4.3 Measurement of Gas Concentration	13
2.4.4 Calculation of Gas Production Rate	14
2.4.5 Calculation of Cumulative Gas Amount	15
2.4.6 Consideration of Henry's Law Equilibrium	15
2.5 Data analysis and Statistics.....	16
3 Results	17
3.1 Soil Characteristics	17

3.1.1	pH Value and Conductivity	17
3.1.2	Water Content and Bulk Density	17
3.1.3	Carbon and Nitrogen Characteristics	18
3.1.4	Grain Size Distribution	20
3.2	Soil Organic Carbon and Nitrogen Stocks and Pools	21
3.3	Radiocarbon Dating and Carbon Accumulation Rates	22
3.4	Incubations – Potential Carbon Release	24
3.4.1	Cumulative CH ₄ Emissions	24
3.4.2	Cumulative CO ₂ Emissions	25
3.4.3	Production Rate of Methane	28
3.4.4	Production Rate of Carbon Dioxide	29
3.5	Relationship between Soil Characteristics and Gas Release	30
4	Discussion	33
4.1	Carbon Characteristics of Active Floodplains	33
4.1.1	Hydrochemical Characterization	33
4.1.2	Grain Size	33
4.1.3	Carbon and Nitrogen Contents	34
4.1.4	Carbon and Nitrogen Stocks and Pools	35
4.1.5	Radiocarbon Ages	36
4.1.6	Accumulation Rates	37
4.2	Potential Carbon Release from Active Floodplains	38
4.2.1	Anaerobic vs. Aerobic Emissions	38
4.2.2	Active vs. Permafrost Layer Emissions	40
4.2.3	Relationship between Soil Characteristics and Carbon Release	40
5	Conclusion	43
	References	XI
	Declaration	XXV

List of Figures

Figure 1 Location of the Lena Delta and the study sites	5
Figure 2 Grain size distribution	20
Figure 3 Cumulative soil organic carbon and soil nitrogen stocks.....	21
Figure 4 Cumulative CH ₄ emissions	25
Figure 5 Cumulative CO ₂ emissions	26
Figure 6 CH ₄ production rate.....	28
Figure 7 CO ₂ production rate.....	29
Figure 8 Summary of soil characteristics and carbon emissions.....	32

List of Tables

Table 1	Description of the analyzed soil cores	8
Table 2	Description of the incubated soil samples	12
Table 3	Soil parameters for the analyzed soil cores	19
Table 4	Soil organic carbon and soil nitrogen stocks	22
Table 5	Radiocarbon ages and accumulation rates	23
Table 6	Cumulative CH ₄ emissions	27
Table 7	Cumulative CO ₂ emissions	27
Table 8	Matrix with correlation coefficient ρ	31

Abbreviations

AD	Anno Domini
a.s.l.	Above sea level
BP	Before present
C	Carbon
cal	Calibrated
C _m	Headspace gas concentration in mass unit
C _v	Headspace gas concentration in parts per million
C/N	Carbon/Nitrogen ratio
F	Mineralization rate
KUR	Kurungnakh
M	Molecular weight
N	Nitrogen
ppm	Parts per million
R	Universal gas constant
SAM	Samoylov
SN	Soil nitrogen
SOC	Soil organic carbon
TC	Total carbon
TN	Total nitrogen
TOC	Total organic carbon
w	Dry mass of soil

1 Introduction

The Arctic is currently experiencing a warming process that is much faster than the average global warming (Trenberth et al., 2007). Therefore, high latitude ecosystems are exposed to drastic changes, which also has an impact on permafrost regions (IPCC, 2022; Serreze et al., 2000). Permafrost is defined as ground that remains at or below 0 °C for two or more consecutive years (van Everdingen, 1998). The perennially frozen soil is covered by an active layer, that thaws during the summer and enables plant growth (mainly mosses, lichens, grasses, dwarf shrubs) and thus is in biogeochemical exchange with the atmosphere (Knoblauch et al., 2013).

According to Zhang et al. (1999), permafrost areas occupy 24% of the land surface in the northern hemisphere. As the frozen state of these soils prevents decomposition processes, permafrost has been storing fossil organic matter since the end of the last ice age or longer (Harden et al., 1992; Schirrmeister et al., 2002; Zimov et al., 2006). It is estimated that northern permafrost regions store ~1300 Pg of soil carbon (Tarnocai et al., 2009; Hugelius et al., 2014), which is about half of the globally stored soil organic carbon and twice the atmospheric C pool (Köchy et al., 2015). Of this, ~472 Pg are stored in the top meter soil and ~822 Pg are stored in the perennially frozen soil (Hugelius et al., 2014).

The warming climate causes permafrost degradation (e.g., Grosse et al., 2011; Romanovsky et al., 2010) by thawing of formerly frozen soil layers, resulting in a deepening of the active layer (Schaefer et al., 2011). This makes large amounts of permafrost soil organic carbon vulnerable to microbial decomposition (Dutta et al., 2006; Schuur et al., 2009), which results in increasing CH₄ and CO₂ release to the atmosphere (Johansson et al., 2006; O'Donnell et al., 2012; Natali et al., 2014), causing a positive feedback to climate change (e.g., Schuur et al., 2009). In addition, changing soil hydrology through thawing of ice rich permafrost influences aerobic and anaerobic conditions, with higher soil moisture favoring anaerobic conditions and thus CH₄ production (Christensen et al., 2004), which has a greater global warming potential than CO₂ (IPCC, 2007). The impact of thawing permafrost soils on carbon release and on the global climate is still highly uncertain (McGuire et al., 2009).

The main Arctic river deltas in permafrost regions occupy only 77,000 km² (Walker, 1998), but play an important role as carbon storages, as the sediment deposits can have a large thickness of up to 60 m due to typical river deltaic sedimentation and accumulation processes (Schwamborn et al., 2002). Moreover, these are highly dynamic environments

at the land-sea interface (Walker, 1998), characterized by active fluvial, deltaic, and permafrost-thaw processes (e.g., periodic flooding, sediment deposition, erosion), which impact the soil carbon (C) and nitrogen (N) stocks (Fuchs et al., 2018). Climate change may intensify these processes, particularly thawing and erosion, which could result in a higher sediment load (Bowden et al., 2008; Lamoureux et al., 2014; Lamoureux & Lafrenière, 2009). A better understanding of these processes will help to improve model estimates for these dynamic permafrost environments.

Active floodplains in Arctic river deltas are understudied, as they consist of sand-rich soils and are expected to not store as large amounts of organic carbon as other geomorphological terraces of the delta (Siewert et al., 2016), even though active floodplains are the dominating unit in the deltas and are highly dynamic due to active erosion and sedimentation by annual spring flooding (Zubrzycki et al., 2013). Only a few studies have focused on carbon and nitrogen stocks and greenhouse gas release from active floodplains within Arctic river deltas. Zubrzycki et al. (2013) studied the SOC and SN stocks and pools of the active floodplains on Samoylov Island in the Lena Delta and Siewert et al. (2016) included alluvial sediments and active floodplains on Kurungnakh Island in the Lena Delta in their study. Further C and N stocks from deltaic deposits in Alaska and Siberia were included by Ping et al. (2011), Hugelius et al. (2011), Hugelius et al. (2014), and Fuchs et al. (2018). There are also few studies on greenhouse gas emissions from active floodplains. Laurent (2021) conducted a short-term incubation at 4 °C and 20 °C with soil samples from various landscape positions on Kurungnakh, including active floodplains. Also, the synthesis of anaerobic incubation studies by Treat et al. (2015) considered study sites within active floodplains. There are long-term incubation studies that did not examine carbon release from active floodplains but did compare mineral and organic permafrost soils as well as aerobic and anaerobic decomposition (e.g., Lee et al., 2012; Knoblauch et al., 2013; Treat et al., 2014), that can be used for a comparison. Even though some incubation studies showed that mineral soils, which include active floodplains, released less carbon than organic soils (e.g., Lee et al., 2012; Treat et al., 2015), there are indications of high CH₄ fluxes in the active floodplains compared to drier sites (Laurent 2021; van Huissteden et al., 2005; Oblogov et al., 2020), highlighting that they deserve more consideration.

However, data on carbon stocks and potential CO₂ and CH₄ release from these dynamic permafrost areas are limited and remain highly uncertain. Therefore, in this study permafrost soil cores of active floodplains in the Lena Delta were analyzed with the aim

(1) to determine SOC and SN stocks down to 1 m depth, (2) to analyze organic carbon and sediment accumulation rates, and (3) to investigate the potential CO₂ and CH₄ release of active floodplain soils. The underlying hypotheses were: the soils are sand-rich and store less organic carbon than other units in the Lena Delta, the active floodplain soils are comparatively young and sedimentation rates are high due to periodic flooding, and emissions are related to soil characteristics (e.g., soil carbon, C/N, and water content) and are higher under aerobic than anaerobic conditions. Therefore, key soil properties, such as pH, conductivity, total organic carbon, total nitrogen, C/N ratio, bulk density, water content, grain size, and radiocarbon ages were determined and a short-term laboratory incubation of active and permafrost layer samples from Kurungnakh and Samoylov Island was performed at 20 °C under aerobic and anaerobic conditions, in order to gain a better understanding of the C accumulation, C Stocks and C emissions from the active floodplains in the Lena Delta.

2 Materials and Methods

2.1 Study Area

The study area is located in the northeastern Siberian Lena River Delta within the continuous permafrost zone in northern Yakutia. The Delta is formed by the Lena River, which discharges into the Laptev Sea (Wetterich et al., 2008; Boike et al., 2019). With 1500 islands and an area of 32,000 km² (Are et al., 2000), the Lena Delta is the largest delta in the Arctic (Boike et al., 2013). The region has an Arctic continental climate with low temperatures and low precipitation (Boike et al., 2019).

The Lena Delta can be classified into three main geomorphological, terrace-like units and the modern floodplains (Grigoriev, 1993; Schwamborn et al., 2002). The floodplains and the youngest unit are of Holocene origin, which is why the latter is also called the Holocene river terrace. It is characterized by polygonal wet tundra with ice wedges and large thermokarst lakes. It covers the central, northern, and eastern parts of the delta (Boike et al., 2013), and the soils are organic-rich sands with silty-sandy peat layers (Schwamborn et al., 2002). According to estimates by Morgenstern et al. (2008), the first terrace and the active floodplains occupy more than half of the delta area (55%).

The second terrace was formed in the late Pleistocene and early Holocene and reaches an elevation of up to 20 m a.s.l. (Schwamborn et al., 2002; Siewert et al., 2016). It is composed of sandy fluvial sediments with low ice contents and large thermokarst lakes and covers the northwestern part of the delta (Boike et al., 2013).

The third and oldest terrace is an erosional remnant from the middle to late Pleistocene. It reaches an elevation of 30 to 55 m a.s.l. (Siewert et al., 2016). The sediment is fine-grained, organic-rich, and ice-rich, and the surface is shaped by polygonal ground and thermokarst processes (Boike et al., 2013).

In this study, the analyzed soil cores are from the active floodplains and were collected on Kurungnakh and Samoylov Island as well as a neighboring island of Samoylov. All the field sites are located in the southern part of the Lena Delta (Figure 1).

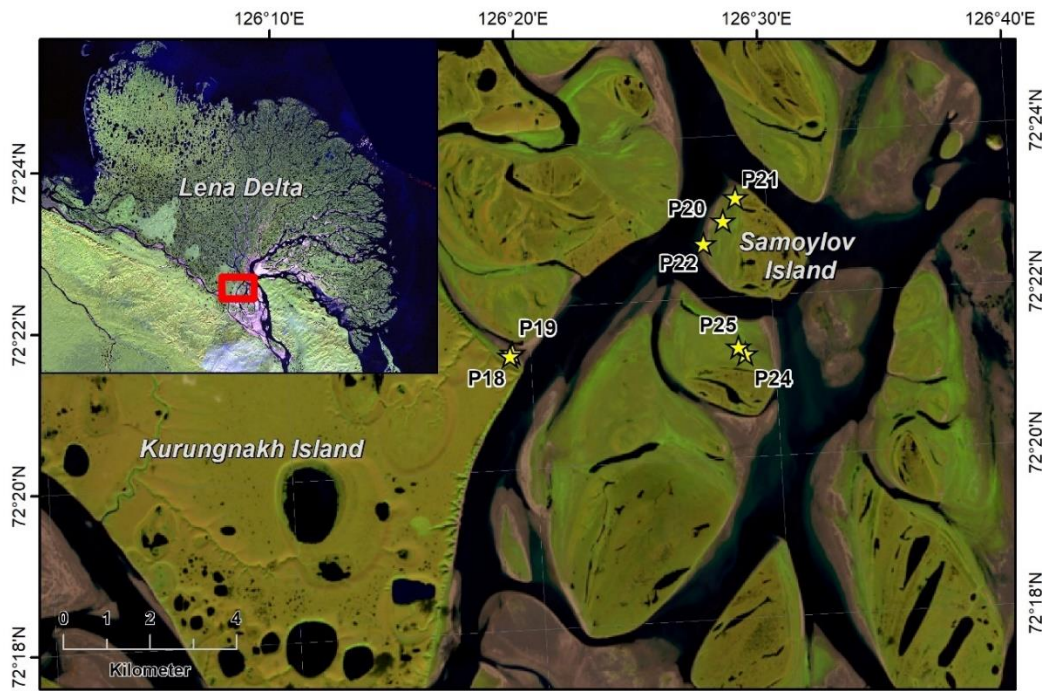


Figure 1 Location of the Lena Delta and the study sites on Kurungnakh Island (P18, P19), Samoylov Island (P20, P21, P22), and the neighboring island of Samoylov (P24, P25) with the corresponding soil cores (Kruse et al., 2019).

Samoylov Island (72°22'N, 126°28'E) is split into the Holocene river terrace and the active floodplain. The eastern part is characterized by ice-wedge polygons with sedge tundra and larger, open or overgrown water bodies (Boike et al., 2019), and has an elevation of 10-16 m a.s.l. (Zubrzycki et al., 2013), while the western part consists of the active floodplains, which are either non-vegetated or with dwarf shrubs dominated tundra (Boike et al., 2019, Siewert et al., 2016) with an altitude of up to 5 m a.s.l. The neighboring island of Samoylov is also part of the active floodplain, which is affected by fluvial sedimentation and is flooded at least once in spring and during high river water levels, whereas the first terrace is flooded only during extreme flooding events (Zubrzycki et al., 2013).

Kurungnakh Island (72°20'N; 126°18'E) is composed of Late Quaternary sediments belonging to the third geomorphological terrace. The island has a stratification consisting of fluvial sandy deposits at the base, overlain by a so-called Ice Complex (ice-rich, silty and peaty deposits with huge ice wedges), and covered by a Holocene layer of silty sands with smaller ice wedges and a polygonal tundra with ponds and thermokarst lakes (Schwamborn et al., 2002; Schirmeister et al., 2003). However, the soil cores analyzed from Kurungnakh belong to the small active floodplain in the Eastern part of the island, which is similar to the cores collected in the floodplains of Samoylov Island and the neighboring island of Samoylov.

The research station on Samoylov has been providing long-term data for climate and soil since 1998 (Boike et al., 2013). Because of the spatial proximity of the sampling sites (Figure 1), these data are also representative for the study areas on Kurungnakh and the neighboring island of Samoylov. The mean annual air temperature from 1998 to 2011 was -12.5 °C. During winter, the temperature can drop below -45 °C and from 1998 to 2011 February was the coldest month with an average temperature of -33.1 °C. In summer, temperatures can reach 25 °C and the warmest month on average from 1998 to 2011 was July with 10.1 °C. The mean annual rainfall in this period was 125 mm, but rainfall occurs only between May and September due to long winters. According to Boike et al. (2013), the mean annual permafrost temperature on Samoylov at a depth of 11 m is about -8.6 °C and the mean thaw depth reaches its maximum of 49 cm in August. Yershov et al. (1991) estimated that the continuous permafrost extends to a depth of 400 to 600 m.

2.2 Site Description, Soil Coring and Sampling

This thesis investigates the carbon characteristics of the active floodplains of the islands described above. In 2018, the Russian-German expedition to Siberia took place, during which 35 soil cores were taken to assess the above-ground and below-ground carbon in the central Lena Delta as part of the KoPf (Kohlenstoff im Permafrost) research project (see Kruse et al., 2019).

The soil coring and sampling was carried out in August 2018 by Matthias Fuchs and Alexandra Runge (both Alfred Wegener Institute, Helmholtz Centre for Polar and Marine Research (AWI), Potsdam). First, the active layers were excavated, described, and sampled with a fixed volume cylinder (250 cm³). Then the permafrost layers were sampled with a modified, snow, ice, and permafrost (SIPRE) auger (Jon Holmgren's Machine Shop, Fairbanks) to a depth of 1 m (core diameter of 7.62 cm) and visually described in their characteristics. Each core was divided into subsamples with 5-10 cm length according to its facies horizons and transported to Alfred Wegener Institute in Potsdam under frozen conditions. Until analysis, the samples were stored at -20 °C (Kruse et al., 2019).

To characterize the active floodplains, the soil cores P18, P19, P20, P21, P22, P24, and P25 (Figure 1) were selected and a total of 48 soil samples were analyzed.¹ All cores represent the low-lying, annually flooded plains, even though they differ in their location,

¹ In addition, data of six samples (P20-1, P20-2, P21-1, P21-2, P22-1, P22-2), which were analyzed in the study of Landgraf (2020), were included in this thesis to complete soil core data.

carbon contents, grain size, moisture conditions and vegetation cover. Table 1 describes the study sites with its corresponding soil cores based on the field observations, with samples from Kurungnakh beginning with KUR18 and samples from Samoylov and its neighboring island beginning with SAM18. Appendix 1 shows photos of the study sites and soil profiles.

2.3 Soil Characteristics

First, standard parameters such as pH, conductivity, and water content were measured, as they may impact the gas production during incubation (Schädel et al., 2020) and are also necessary for further calculations. The total carbon (TC), total organic carbon (TOC), and total nitrogen (TN) were measured to calculate the carbon and nitrogen stocks as well as the gas production rates during incubation. Grain size and radiocarbon ages were determined to investigate accumulation processes.

For this analysis, subsamples were prepared by splitting the frozen soil samples with a cleaned hammer and chisel in a climate chamber at -4 °C. One subsample was used to determine pH, conductivity, water content, grain size, TOC, TC and TN, while another subsample was used for incubations.

2.3.1 pH Value and Electric Conductivity

For hydrochemical characterization, pH and electrical conductivity of the soil pore water were measured. Frozen subsamples were thawed in plastic bags at 4 °C overnight. The pore water was extracted from the soil using rhizon soil moisture samplers. Rhizons are tubes of 5 or 10 cm length with a hydrophilic, porous polymer surface with a pore diameter of 0.1 to 0.2 μm (Meijboom & van Noordwijk 1991). For preparation, the thawed soil was mixed by kneading the bags. To ensure that the rhizon had been surrounded by water, the bags were compressed by tape, especially for drier samples, and the opening of the bags was sealed with tape to prevent water loss. A syringe was connected, drawn up and fixed with a wooden spatula. The resulting vacuum leads to pore water absorption (Appendix 2). At least 4 ml of pore water is required for the measurement, thus sampling time ranged from a few minutes to several hours, depending on the water content of the sample. Measurements were performed with the WTW Multi 540, and conductivity was measured first since the pH meter is stored in KCl solution.

Table 1 Description of soil cores P18, P19, P20, P21, P22, P24, and P25 in their location, number of samples per core, core depth, active layer thickness, soil texture and vegetation. Description is based on field observations by Matthias Fuchs (AWI Potsdam). Photos of study sites and soil profiles in Appendix 1.

Core Name	Location	Number of Samples	Core Depth [cm]	Active Layer Depth [cm]	Soil Description	Surface Description
KUR18-P18	Kurungnakh	5	69	105	dark and light brown sand with peat layers	sandbank, no vegetation, driftwood
KUR18-P19	Kurungnakh	9	112	82	silty sand/sandy silt, rooted, org. inclusions	grasses, shrubs, <i>Equisetum</i> , driftwood
SAM18-P20	Samoylov	9	114.5	82	light/dark gray sand, rooted, silty sand with organic inclusions	shrubs, <i>Equisetum</i> , mosses
SAM18-P21	Samoylov	9	104.5	57	organic rich sandy silt, rooted, sandy layers, org. inclusions	<i>Equisetum</i> , grasses, shrubs, mosses, driftwood
SAM18-P22	Samoylov	5	66	> 1	sand without layers	sandbank, no vegetation, some grasses
SAM18-P24	neighboring island	8	95	54	sandy silt, rooted, organic rich and sandy layers	shrubs, <i>Equisetum</i> , sedges, mosses
SAM18-P25	neighboring island	9	102	59	organic rich silt with roots and sand layers	<i>Dryas</i> , <i>Salix</i> , grasses, mosses, driftwood

2.3.2 Water Content

The subsamples were freeze-dried and weighed before and after the freeze-drying process to determine the water content.² The absolute water content was calculated based on the weight difference (Eq. 1). The results are given in weight percent (wt%).

$$\theta_w = \frac{\text{wet weight} - \text{dry weight}}{\text{wet weight}} \quad \text{Eq. 1}$$

θ_w : absolute water content [wt%]

wet weight: weight of frozen sample [g]

dry weight: weight of freeze-dried sample [g]

2.3.3 Grain Size

The grain size distribution of the samples was determined, which helps identifying stratigraphic layers and deducing sedimentary processes. For preparation, the freeze-dried samples were mixed and subsampled. About 30 g of each sample was weighed into a beaker and 100 ml of 3% hydrogen peroxide (H₂O₂) was added in order to decompose organic remnants. The inorganic fraction, which is relevant for grain size analysis, was not decomposed and remained. To accelerate the reaction, beakers were placed on a heated platform shaker (60 °C, Edmund Bühler GmbH) for about three weeks. During this time, H₂O₂ was added daily and the pH was hold in a neutral range with ammonia (NH₃) and acetic acid (CH₃COOH) to avoid decomposition of inorganic components caused by an acidic environment.

Then, samples were centrifuged several times (Thermo Scientific Heraeus Cryofuge 8500i Centrifuge; Thermo Scientific Heraeus Megafuge 40 Centrifuge) to remove remaining H₂O₂, NH₃, CH₃COOH, and water. After freeze-drying the inorganic residue, 1-3 grams of sample were weighed into a plastic bottle, a dispersant (tetra-sodium pyrophosphate 10-hydrate) and distilled water were added. By placing the plastic bottles in an overhead shaker for 24 hours, a hydrate shell formed around the grains. After that the particle size distribution of each sample was determined with Malvern Mastersizer 3000 laser particle sizer (settled at 2 mm). The instrument gave the results in grain size classes and the corresponding volume fractions in percent (vol%). The classification was made according to DIN 4022 (sand: 0.06-2.0 mm; silt: 0.002-0.06 mm; clay: < 0.002 mm). Statistics were calculated using GRADISTATv 9.1 (Blott 2001).

² In the following chapters "Ice Content" will be referred to as "Water Content", even if it is frozen.

2.3.4 Carbon and Nitrogen Analysis

The carbon and nitrogen characteristics are relevant in terms of potential greenhouse gas release when permafrost soils thaw (Hobbie, 2000). The decomposition of organic matter depends on the amount and lability of carbon, expressed by TOC and C/N (Schädel et al., 2014). Therefore, TC, TOC, and TN of the soil samples were quantified.

Subsamples were taken from the freeze-dried samples and milled with the Pulverisette 5 planetary mill (FRITSCH) (360 rotation rounds per minute, 8 minutes). Afterward, samples (double determination) and corresponding standards and blanks were weighed into crucibles and TC, TOC, and TN were determined with the C analyzer soli TOC cube and the N analyzer rapid MAX N exceed (both from elementar), respectively. The resulting TC, TOC, and TN values were presented as weight percent (wt%).

2.3.5 Organic Carbon and Total Nitrogen Stocks

The soil organic carbon and soil nitrogen stocks were calculated according to Michaelson et al. (1996). First, the carbon and nitrogen density in g cm^{-3} was calculated by multiplying the dry bulk density with the TOC and TN contents. Since the dry bulk density could not be calculated by dividing the dry weight of the sample by the initial volume of the sample, it was calculated using the absolute water content according to Fuchs (2019), who examined the relationship between water content and dry bulk density in his study (Appendix 3). Storages in kg m^{-2} were calculated by multiplying carbon or nitrogen density with the sample length in cm. Missing soil core intervals were extrapolated from the stocks of the respective overlying and underlying layers with same or similar sedimentary characteristics (based on field notes). The stocks were then added up to the reference depths of 0-30 cm and 0-100 cm.

2.3.6 Carbon and Nitrogen Pools of Active Floodplains

The soil organic carbon and soil nitrogen pools of the active floodplains in the Lena Delta were estimated by upscaling the SOC and SN stocks of the analyzed soil cores. For this, the mean SOC and SN stocks of all seven cores and for all reference depths (0-30 cm, 0-100 cm) were multiplied by the area of the active floodplains in the entire Lena Delta. According to satellite image classification by Zubrzycki et al. (2013), the active floodplains are the dominating unit in the Lena Delta, occupying an area of about 8830 km^2 , which is approximately 40% of the land-covered area.

2.3.7 Radiocarbon Dating

Radiocarbon dating was performed for age determination in order to assess the carbon and sediment accumulation processes. However, this was only done for the soil cores P19, P24, and P25 at six depths, firstly, because these cores were also incubated, secondly, because of limited laboratory capacity. For this, plant remains in the freeze-dried samples were handpicked under the microscope. It is important to select material that has grown directly on the sites, e.g., sedge leaves. Wood, for example, may have been washed up and thus falsify the radiocarbon dating. The plant remains were weighed and then analyzed using the Mini Carbon Dating System (MICADAS) based on accelerator mass spectrometry (AMS) at Alfred Wegener Institute in Bremerhaven (Mollenhauer et al., 2021).

The radiocarbon ages were calibrated with CALIBomb software (Reimer & Reimer, 2022) using IntCal20 calibration curve and $F^{14}C$ as reference (recommended for post-bomb samples by Reimer et al. (2004)). The calibrated ages are given in calibrated years before present (cal yr BP) and calibrated years Anno Domini (cal yr AD).

2.3.8 Carbon and Sediment Accumulation Rates

Based on the radiocarbon ages, the mean carbon accumulation rates in $g\ C\ m^{-2}\ year^{-1}$, as well as the sediment accumulation rates in $mm\ year^{-1}$ were determined according to Fuchs et al. (2018). For calculating the mean carbon accumulation rate, the soil organic carbon of each core was summed to the depth of the radiocarbon sample and then divided by the number of years between sampling year and the calibrated age of each sample. The episodic accumulation rate was calculated similarly but represents the rates between two samples. In addition, the mean sediment accumulation rate was calculated by dividing the sediment height from the mean depth of each sample to the surface by the number of years between sampling year and calibrated sample age (Fuchs et al., 2018).

2.4 Incubation Experiment

The potential release of CO₂ and CH₄ due to microbial degradation of organic matter was investigated by thawing the frozen soil samples in an incubation experiment. Since it was a short-term incubation, information about the immediately available carbon is provided. If the experiment were continued, it would also be possible to draw conclusions about the carbon pools, which are converted more slowly. Both help to understand the carbon cycle of ecosystems (Robertson et al., 1999) and give a first indication about the carbon release potential in permafrost-affected floodplains.

2.4.1 Description of Incubated Samples

In total 36 subsamples from three cores P19, P24 and P25 were incubated under aerobic and anaerobic conditions and at two depths each, representing the active layer and the permafrost layer.³ P19 is located in the Eastern part of Kurungnakh, whereas P24 and P25 are close to each other on the neighboring island of Samoylov (Figure 1). These three cores were collected, because they are representative for the active floodplains.

The samples for the active and the permafrost layer of each core were selected according to comparable depths, but different characteristics in terms of water content, TOC, and grain size by using the field notes and first results of the soil analysis. The following table 2 shows the geochemical characteristics of the incubated samples.

Table 2 Incubated samples of the cores P19, P24 and P25 at comparable depths for active and permafrost layer, but different water content, organic carbon, and soil texture (according to sand/silt/clay triangle of grain size analysis).

Sample Name	Sample Depth [cm]	Water Content [wt%]	TOC [wt%]	Soil Texture
P19 – active layer	23-30	16.8	0.337	sand
P19 – permafrost layer	82-87	34.5	1.564	silty sand
P24 – active layer	25-32	47.0	4.566	sandy silt
P24 – permafrost layer	75.5-82	34.3	1.394	silty sand
P25 – active layer	27-35	16.7	0.164	sand
P25 – permafrost layer	85-90	17.1	0.178	sand

³ In the following, the term "permafrost layer" always refers to the frozen soil horizon and its samples.

2.4.2 Incubation Setup

Incubations were performed under both aerobic and anaerobic conditions. One sample of the active layer and one sample of the permafrost layer were incubated per core and there were three replicates per sample, resulting in 36 incubated soil samples (18 aerobic, 18 anaerobic). In addition, two blanks were included per treatment.

For preparations, subsamples from the frozen soil samples were thawed in closed plastic bags over night in a cooling room at 4 °C. The next day, thawed subsamples were homogenized by kneading the bags and around 15 g were weighed into 120 ml vials for all 36 soil incubations. For anaerobic incubations, this was done in a glovebox with an anoxic atmosphere (N₂), whereas the aerobic incubation samples were prepared at ambient air. The aerobic samples were kept at field moisture conditions, whereas sterilized water was added to the anaerobic ones when water content was less than 30% to achieve soil saturation, while keeping the effect of gas dissolution low (Appendix 4: Calculation of added water).

All vials were permanently closed with airtight lids (rubber stopper and aluminum lids) to create and maintain both anoxic conditions and constant humidity in the anaerobic incubations as well as aerobic, CO₂-free conditions and constant humidity in the aerobic incubations. The closed vials were stored at 1 °C over night to avoid the onset of microbial activity. The next day, the headspace of the vials was flushed to perform the first gas concentration measurement of t₀. Anaerobic incubations were flushed with N₂ for three minutes to remove the remaining O₂, whereas aerobic incubations were flushed with synthetic, CO₂-free air (20% O₂, 80% N₂). Afterward, samples were brought to incubation temperature. Incubations were performed over 10 weeks in the dark in an incubator at a constant temperature of 20 °C. This incubation temperature was chosen to avoid microorganisms remaining in a long lag phase during the short-term experiment as observed in an incubation study at 4 °C by Laurent (2021).

2.4.3 Measurement of Gas Concentration

The CO₂ and CH₄ concentrations were determined by gas chromatography (7890A, Agilent Technologies, USA) at the German Research Centre for Geosciences (GFZ), Potsdam. Gases were separated on an Agilent 19095P-QO4 column and quantified with a flame ionization detector (FID). The column temperature was 50 °C and helium served as a carrier gas, with a flow of 15 mL min⁻¹ and a runtime of 4.5 minutes.

Before each measurement, the rubber stopper was sterilized by inflaming with 99% ethanol and 350 μL from the headspace gas were taken manually with a Hamilton gastight syringe and a sterile needle (Appendix 5). After the injection needle was attached and flushed with 100 μL of gas sample, the remaining 250 μL were injected into the gas chromatograph (GC).

For both incubation types, measurements were taken every second day in the first two weeks, then twice per week for two weeks and then weekly for the last six weeks. When CO_2 concentration exceeded 10,000 ppm during the measurement period, the headspace was flushed with synthetic air (20% O_2 , 80% N_2) for the aerobic incubations and with N_2 for the anaerobic ones to avoid gas saturation (Appendix 5). In case of flushing, the gas concentration was measured both before and after flushing for later calculations.

2.4.4 Calculation of Gas Production Rate

The gas production rate was calculated according to Robertson et al. (1999) by using the change in headspace CO_2 and CH_4 concentration over time.

First, the CO_2 and CH_4 concentrations, which were given by the GC in parts per million (ppm), were converted to mass units ($\mu\text{g L}^{-1}$) and corrected for incubation conditions by applying the Ideal Gas Law.

$$C_m = \frac{C_v \cdot M \cdot P}{R \cdot T} \quad \text{Eq. 2}$$

C_m : headspace gas concentration in $\mu\text{g CO}_2\text{-C/L}$; C_v : headspace gas concentration in ppm_v CO_2 or CH_4 ; M : molecular weight of $\text{CO}_2\text{-C}$ or $\text{CH}_4\text{-C}$ ($12\mu\text{g } \mu\text{mol}^{-1}$); P : barometric pressure (1 atm); R : universal gas constant $0.0820575 \text{ L atm K}^{-1} \text{ mol}^{-1}$; T : incubation temperature ($^\circ\text{Kelvin}$)⁴

Then, the change in gas concentration (C_{rate}) between two measurement days (t_x and t_{x+1}) was calculated by linear regression.

$$C_{rate} = \frac{C_{tx+1} - C_{tx}}{t_{x+1} - t_x} \quad \text{Eq. 3}$$

⁴ For simplicity, this chapter always refers to the unit in $\mu\text{g CO}_2\text{-C}$, even though the calculations were also performed for methane in $\mu\text{g CH}_4\text{-C}$.

Next, the normalized mineralization rate F was calculated with the following formula (Eq. 4). Depending on whether one divides by dry mass and initial carbon or only by dry mass, F is obtained in $\mu\text{g CO}_2\text{-C per gram of soil carbon } (\mu\text{g CO}_2\text{-C gC}^{-1}\text{d}^{-1})$ or $\mu\text{g CO}_2\text{-C per gram of dry soil } (\mu\text{g CO}_2\text{-C gsoil}^{-1}\text{d}^{-1})$, respectively. The mineralization rate F was calculated in both units.

$$F = \frac{C_{rate} \cdot V}{TC \cdot W} \quad \text{Eq. 4}$$

F : C mineralization rate ($\mu\text{g CO}_2\text{-C gC}^{-1}\text{d}^{-1}$); C_{rate} : change in gas concentration between two measurements ($\mu\text{g CO}_2\text{-C L}^{-1}\text{headspace}^{-1}\text{d}^{-1}$); W : dry mass inside the vial (g); TC : initial carbon (gram dry weight)

Last, the mean of the replicates per core and layer (active and permafrost) was calculated.

2.4.5 Calculation of Cumulative Gas Amount

The calculation of the cumulative gas emissions within 10 weeks was done as in Equation 4, but C_{rate} was replaced by gas concentration C_m to obtain the gas amount in $\mu\text{g CO}_2\text{-C gC}^{-1}$ and $\mu\text{g CO}_2\text{-C gsoil}^{-1}$ for each measurement day. The differences between the gas concentrations of two measurement days were added to obtain the cumulative emissions over 10 weeks of incubation.

2.4.6 Consideration of Henry's Law Equilibrium

Due to Henry's law, which describes the solubility behavior of gases in a liquid, part of the gas is dissolved in the water phase. This means that the actual gas concentration was greater than measured in the headspace gas. Even if the water content in the samples was very small, the dissolved gas concentration was calculated and the headspace concentration was corrected. For the calculation, the dimensionless Henry's law solubility constants H^{cc} of CH_4 and CO_2 from Sander (2015) were used. In Sander (2015) they are given as H^{cp} in $\text{mol m}^{-3} \text{Pa}^{-1}$ at 25°C . Therefore, the constants were converted both to the incubation temperature of 20°C and from H^{cp} to H^{cc} . Equation 5 was used to convert to incubation temperature.

$$kH_{cp} = kH_{cp\theta} \cdot \exp\left(C \cdot \left(\frac{1}{T_{inc}} - \frac{1}{T_\theta}\right)\right) \quad \text{Eq. 5}$$

kH_{cp} : Henry constant at incubation temperature in $\text{mol L}^{-1}\text{atm}^{-1}$; $kH_{cp\theta}$: Henry constant at reference temperature in $\text{mol L}^{-1}\text{atm}^{-1}$; C : constant describing temperature dependence [K]; T_{inc} : incubation temperature in Kelvin; T_θ : reference temperature in Kelvin.

2.5 Data analysis and Statistics

Calculations, statistical tests, and plotting were done with Microsoft Excel (version 2201) and R Studio (version 2021.09.1+372). To determine correlations between soil properties as well as soil properties and emissions, the non-parametric Spearman correlation coefficient was used. To analyze significant differences between the soil cores, layers, and treatments in the incubation experiment, ANOVA (one-way analysis of variance) and a pairwise post-hoc test (Tukey) were performed for the core comparison. For comparison of layers and treatments, t-tests were performed. These statistical tests were selected even when there was no normal distribution because they provided more reliable results compared with the non-parametric Mann-Whitney U test. Since the lack of normal distribution was probably due to the small sample size, it was assumed that the data would be normally distributed if the sample size were larger.

3 Results

3.1 Soil Characteristics

The soil parameters pH value, conductivity, water content, bulk density, total organic carbon, total nitrogen, and C/N ratio are described below and are summarized in table 3 for the active and the permafrost layer of each core. Additionally, Appendix 6 details the results for all 48 analyzed samples and the six samples of Landgraf (2020). For simplicity, "KUR18" and "SAM18" are not always mentioned in the core names.

3.1.1 pH Value and Conductivity

The pH value was in a neutral range for all 48 samples, averaging 7.33 ± 0.28 . No general trend was observed with depth and when comparing the active and permafrost layer. However, the permafrost layers of the soil profiles P19 and P20 showed lower pH values than their corresponding active layers and all other samples, averaging 6.90 ± 0.04 and 6.89 ± 0.03 , respectively. The conductivity ranged from $110 \mu\text{S cm}^{-1}$ to $529 \mu\text{S cm}^{-1}$. Only the samples P24-1 and P25-1 (each the closest to the surface) were exceptions and outside this range with $914 \mu\text{S cm}^{-1}$ and $1342 \mu\text{S cm}^{-1}$, respectively.

3.1.2 Water Content and Bulk Density

The water content of all samples ranged between 8% and 47%, averaging $29 \pm 10\%$. The active layers of the sandbank cores P18 and P22 had the lowest water contents, averaging $20 \pm 4\%$ and $16 \pm 5\%$, respectively. The overall highest water contents were in the permafrost layer of P20 and the active layer of P24, with $40 \pm 8\%$ and $40 \pm 0.1\%$, respectively. There was no general trend between active and permafrost layer. For P24 and P25, the water content in the active layer was higher than in the permafrost layer, whereas for P19 and P20 it was the opposite. Only core P22 showed a continuous increase in water content with depth, the other cores did not show a clear trend. The dry bulk density correlated with the water content and decreased with increasing water content, as a result of the calculation method for dry bulk density based on the water content. It ranged between 0.64 g cm^{-3} and 1.64 g cm^{-3} and was on average $1.07 \pm 0.24 \text{ g cm}^{-3}$.

3.1.3 Carbon and Nitrogen Characteristics

The TOC content ranged from 0.11% to 7.39% and generally varied between cores and with depth, with an average of $1.75 \pm 1.53\%$ for all samples. For the first two samples of P22, the TOC was below the detection limit (TOC < 0.10 %), thus an estimated value of 0.05% was assumed for further calculations of carbon stocks. The cores P18 and P22 from the sandbanks had on average the lowest TOC values, whereas the active layer of P24 and P25 had the highest TOC (Table 3). A difference between active and permafrost layer or a trend with depth was only observed in P24 and P25. Here, the TOC generally decreased with depth (detailed data in Appendix 6).

Overall, the TN contents were very low, averaging $0.16 \pm 0.06\%$ for all samples (assuming TN = 0% when TN was below detection limit of 0.10%). Samples with TN below the detection limit occurred in all cores (Table 3; Appendix 6), but in P18 and P22 all samples were below the detection limit.

The C/N ratio ranged from 14.37 to 24.75, with the highest ratios occurring in P24, where active and permafrost layers averaged 22.58 ± 1.55 and 24.33 ± 0.00 , respectively. The lowest ratio occurred in the permafrost layer of P19 with an average of 14.74 ± 0.20 (Table 3). In samples with TN or TOC below detection limit, the C/N ratio was not calculated, and the corresponding samples were not included in the average of the active and permafrost layers.

Table 3 Soil parameters for the analyzed cores, given as the mean of active and permafrost layer samples for each core and corresponding standard deviations (detailed table for all analyzed samples in Appendix 6).

Sample	Layer	Core Depth [cm]	Number of Samples	pH [-]	Conductivity [$\mu\text{S cm}^{-1}$]	Water Content [wt%]	Dry Bulk Density [g cm^{-3}]	TOC [wt%]	TN [wt%]	C/N [-]
KUR18-P18	active	69	5	7.38 ± 0.23	226 ± 85	20 ± 4	1.28 ± 0.12	0.49 ± 0.35	-	-
KUR18-P19	active	80	6	7.43 ± 0.35	303 ± 57	28 ± 7	1.08 ± 0.19	1.64 ± 0.95	0.09 ± 0.07	15.55 ± 0.85
KUR18-P19	permafrost	112	3	6.90 ± 0.04	269 ± 84	37 ± 2	0.85 ± 0.05	1.51 ± 0.36	0.08 ± 0.06	14.74 ± 0.20
SAM18-P20	active	81	6	7.18 ± 0.08	189 ± 45	25 ± 5	1.14 ± 0.14	1.37 ± 0.62	0.07 ± 0.05	15.97 ± 1.34
SAM18-P20	permafrost	114.5	3	6.89 ± 0.03	261 ± 14	40 ± 8	0.79 ± 0.17	2.42 ± 0.88	0.12 ± 0.09	16.41 ± 0.09
SAM18-P21	active	50	5	7.31 ± 0.11	441 ± 79	34 ± 7	0.93 ± 0.17	2.53 ± 1.09	0.14 ± 0.08	16.55 ± 1.41
SAM18-P21	permafrost	104.5	4	7.25 ± 0.18	230 ± 96	32 ± 11	0.99 ± 0.25	1.50 ± 1.13	0.09 ± 0.09	15.14 ± 0.67
SAM18-P22	active	66	5	7.51 ± 0.12	208 ± 32	16 ± 5	1.41 ± 0.14	0.16 ± 0.19	-	-
SAM18-P24	active	47	4	7.32 ± 0.22	487 ± 271	40 ± 6	0.80 ± 0.13	3.71 ± 1.43	0.14 ± 0.09	22.58 ± 1.55
SAM18-P24	permafrost	95	4	7.36 ± 0.24	241 ± 79	28 ± 7	1.07 ± 0.18	1.25 ± 1.02	0.03 ± 0.05	24.33 ± 0.00
SAM18-P25	active	53	5	7.58 ± 0.08	469 ± 446	31 ± 10	1.02 ± 0.24	3.07 ± 2.71	0.16 ± 0.15	18.52 ± 0.51
SAM18-P25	permafrost	102	4	7.56 ± 0.22	193 ± 18	25 ± 5	1.16 ± 0.13	1.01 ± 0.72	0.03 ± 0.05	20.20 ± 0.00

3.1.4 Grain Size Distribution

According to the analysis of the grain size data with GRADISTATv (Blott, 2001), the samples were assigned to the textural groups sand, sandy silt, or silty sand. For all 48 samples, the average percentages of sand, silt and clay were 70.8%, 26.1%, and 3.1%, respectively. Overall, the sand content ranged from 24.5% to 99.4%, the silt content was between 0.5% and 66.9%, and the clay fraction was lowest with 0% to 8.6%. Cores P18 and P22 from non-vegetated sandbanks had high sand contents in all depths. As figure 2 shows, in all cores the grain size distribution varied with depth and sandy or silty layers were identified (e.g., sandy layers in P19 at a depth of 23-47 cm and in P21 at a depth of 60-81 cm). The cores P24 and P25 showed a trend of an increasing sand fraction and a decreasing silt fraction with depth (Figure 2). In addition, grain-size distribution is very poorly to well sorted (according to Folk and Ward, 1957) with a mix of unimodal, bimodal, trimodal, and polymodal distribution curves. While unimodal distributed grain-size curves usually had one major peak in the sand fraction, bimodal, trimodal and polymodal curves mostly had another peak or at least a higher proportion in the silt fraction. Appendix 7 contains detailed information about grain size distribution for all 48 analyzed samples.

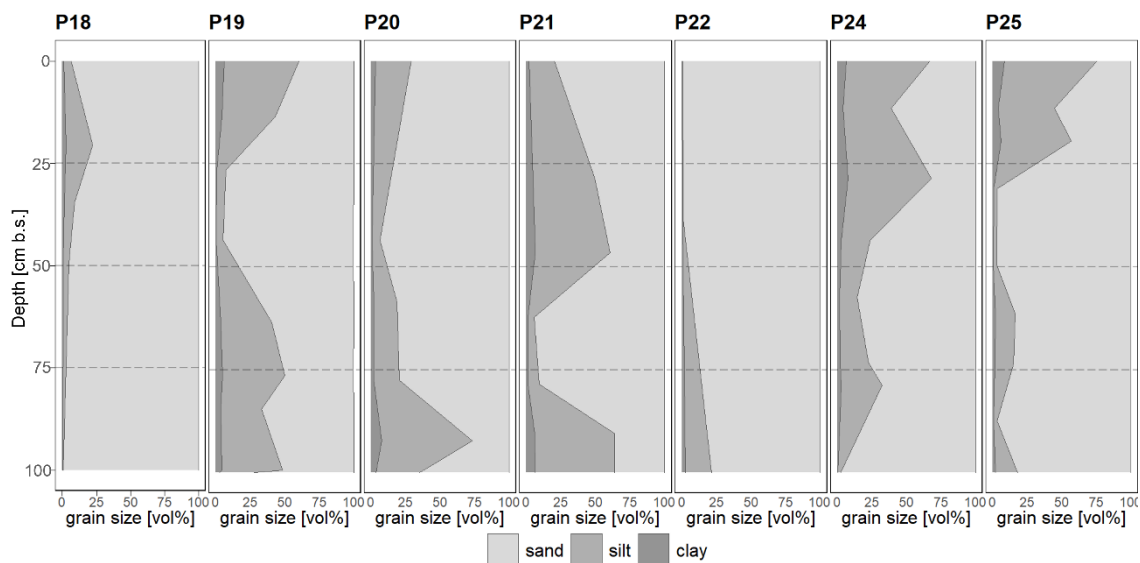


Figure 2 Grain size distribution against depth below surface (b.s.) from 0 to 100 cm, given in volume percent (vol%); each value is given at the mean depth of each sample, in between a linear gradient was assumed.

3.2 Soil Organic Carbon and Nitrogen Stocks and Pools

Stocks were calculated for the first meter of soil and ranged for SOC between 3.10 and 19.45 kg C m⁻² (0-100 cm) (Table 4). The mean SOC stock of all cores for the first meter soil was 12.89 ± 6.02 kg C m⁻², with around 40% stored in the first 30 cm. P18 and P22 had the lowest carbon stocks, while P19, P20, and P25 stored a similar amount of carbon, and P24 and P21 had the highest carbon stocks (Figure 3). When excluding the soil profiles P18 and P22 of the non-vegetated sandbanks, the mean SOC stock of the vegetated active floodplains was 16.53 kg C m⁻² (0-100 cm). According to estimates by Zubrzycki et al. (2013), the active floodplains occupy an area of 8830 km² in the Lena Delta. When extrapolating the average of 12.89 ± 6.02 kg C m⁻², the total carbon pool was estimated to be 114 ± 53 Tg C for the first meter of soil.

The nitrogen stocks of the cores were much lower, ranging from 0.61 to 1.07 kg N m⁻². The mean N stock of all cores was 0.56 ± 0.38 kg N m⁻² (0-100 cm), with around 42% stored in the first 30 cm. Stocks were not calculated for P18 and P22, because the TN contents of all their samples were below the detection limit (< 0.10%) and an assumption of TN = 0.05% would presumably have led to an overestimation of the stocks. When the soil profiles P18 and P22 of the non-vegetated sandbanks were not considered, the mean N stock of the vegetated active floodplains was 0.79 kg N m⁻² (0-100 cm). When extrapolating the average of 0.56 ± 0.38 kg C m⁻² based on the above-mentioned area of 8830 km², the total nitrogen pool of the active floodplains in the entire Lena Delta was about 5 ± 3 Tg N (0-100 cm).

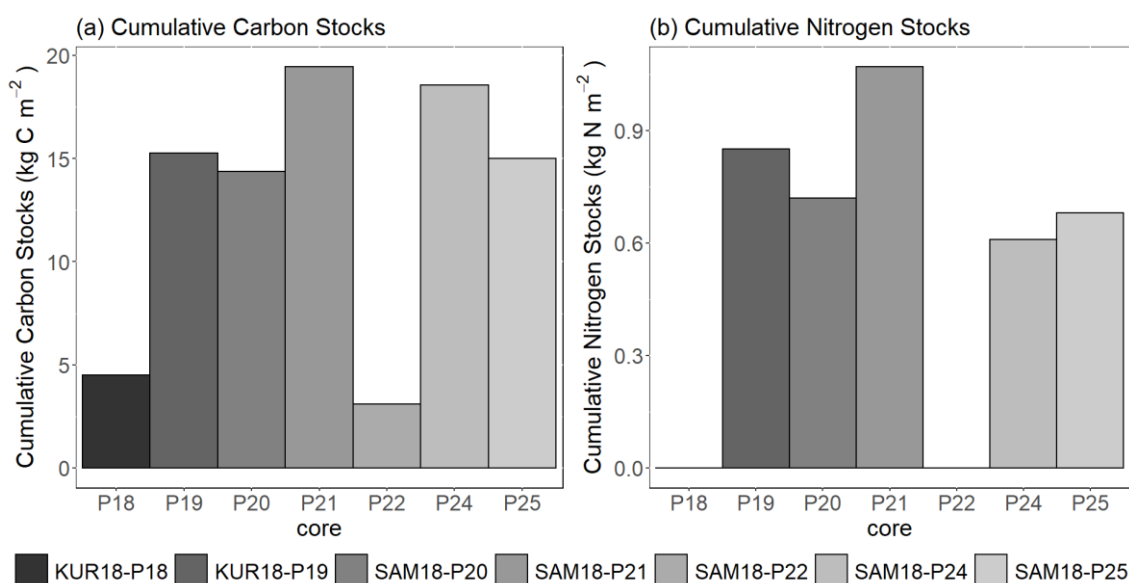


Figure 3 Cumulative soil organic carbon stocks in kg C m⁻² (a) and soil nitrogen stocks in kg N m⁻² (b) for a reference depth of one meter; for samples with TN content below detection limit of element analyzer, TN was assumed to be 0%.

Table 4 Soil organic carbon (SOC) and soil nitrogen (SN) stocks for the seven soil cores for commonly used reference intervals of 0-30 cm and 0-100 cm. SOC stocks are given in kg C m⁻² and SN stocks are given in kg N m⁻²; for samples with TN content below detection limit of element analyzer, TN was assumed to be 0%.

Core Name	SOC Stocks [kg C m ⁻²]		SN Stocks [kg N m ⁻²]	
	0-30 cm	0-100 cm	0-30 cm	0-100 cm
KUR18-P18	2.35	4.50	-	-
KUR18-P19	4.91	15.25	0.30	0.85
SAM18-P20	3.37	14.37	0.09	0.72
SAM18-P21	6.67	19.45	0.32	1.07
SAM18-P22	0.26	3.10	-	-
SAM18-P24	8.98	18.56	0.40	0.61
SAM18-P25	9.83	15.01	0.53	0.68

3.3 Radiocarbon Dating and Carbon Accumulation Rates

Radiocarbon dating as well as carbon and sediment accumulation rates were determined for selected layers of the cores P19, P24, and P25, which were incubated. Table 5 shows the calibrated ages in years before present (cal yr BP) and years anno domini (cal yr AD) for the corresponding samples and depths as well as the accumulation rates of organic carbon and sediment. The ages of all samples ranged from 360 ± 52 to 2016 ± 2 cal yr AD, which indicated very young material in the floodplains. In comparison, the soil profile P19 had the youngest layers and showed two age inversions. For profiles P24 and P25, the age decreased with depth, reaching up to 360 ± 52 cal yr AD and 365 ± 61 cal yr AD in the deepest layers, respectively.

The carbon accumulation rates ranged from $9.23 \text{ g C m}^{-2} \text{ yr}^{-1}$ to $320.62 \text{ g C m}^{-2} \text{ yr}^{-1}$. The two age-inversed samples from P19 had carbon accumulation rates up to $767.66 \text{ g C m}^{-2} \text{ yr}^{-1}$ and $4687.92 \text{ g C m}^{-2} \text{ yr}^{-1}$, and were likely exceptions or outliers. When excluding the outliers, the mean carbon accumulation rate for all samples was at $161.54 \pm 124.25 \text{ g C m}^{-2} \text{ yr}^{-1}$. The sediment accumulation rate ranged between 0.44 mm yr^{-1} and 20.23 mm yr^{-1} and was on average $6.89 \pm 6.09 \text{ mm yr}^{-1}$, when excluding the age-inversed samples of P19 with 50.59 mm yr^{-1} and $306.02 \text{ mm yr}^{-1}$. Table 5 also lists the episodic carbon and episodic sediment accumulation rates.

Table 5 Dated samples with calibrated radiocarbon ages (¹⁴Chrono intcal20 software (Reimer & Reimer., 2022)), mean organic carbon and mean sediment accumulation rates, and episodic organic carbon and episodic sediment accumulation rates; modern radiocarbon dates indicate a negative calibrated age.

Sample Name	Layer	Depth [cm]	F ¹⁴ C [-]	Cal age [years BP]	Cal age [years AD]	Cum SOC [kg C m ⁻²]	Mean OC acc rate [g C m ⁻² yr ⁻¹]	Episodic OC acc rate [g C m ⁻² yr ⁻¹]	Mean sediment acc rate [mm yr ⁻¹]	Episodic sediment acc rate [mm yr ⁻¹]
KUR18-P19-3	active	26.5	1.2637 ± 0.0076	-31 ± 1.0	1981 ± 1	4.91	132.91	132.91	7.17	7.17
KUR18-P19-5	active	63.5	1.0209 ± 0.0039	0 ± 0.0	2016 ± 2	9.73	4687.92	NA	306.02	NA
KUR18-P19-7	permafrost	84.5	1.352 ± 0.0102	-27 ± 1.0	1976 ± 1	13.33	320.62	91.29	20.32	5.31
KUR18-P19-9	permafrost	109.25	1.1141 ± 0.0068	-46 ± 2.6	1996 ± 3	16.58	767.66	NA	50.59	NA
SAM18-P24-3	active	28.5	1.2415 ± 0.0050	-33 ± 0.9	1983 ± 1	9.58	272.25	272.25	8.10	8.10
SAM18-P24-4	active	43.5	1.4241 ± 0.0111	-24 ± 1.0	1974 ± 1	13.18	298.23	399.59	9.84	16.64
SAM18-P24-6	permafrost	73.25	0.8072 ± 0.0033	1590 ± 52.3	360 ± 52	17.09	10.31	2.42	0.44	0.18
SAM18-P25-4	active	31	1.4599 ± 0.0049	-22 ± 0.4	1972 ± 0	9.94	218.24	218.24	6.81	6.81
SAM18-P25-8	permafrost	87.5	0.967 ± 0.0043	402 ± 53.1	1548 ± 53	14.35	30.56	10.41	1.86	1.33
SAM18-P25-9	permafrost	100	0.8094 ± 0.0040	1585 ± 61.3	365 ± 61	15.26	9.23	0.77	0.61	0.11

3.4 Incubations – Potential Carbon Release

Below, the cumulative CH₄ and CO₂ emissions as well as the daily production rates under anaerobic and aerobic conditions during the 68-day incubation are presented. They are expressed in two different units (see chapter 2.4.5): (1) per gram of dry soil, which provides information on the quantitative carbon release, and (2) per gram of soil carbon, which shows the qualitative nature and decomposability of the stored carbon independent of its concentration (Lee et al., 2012). The production rates are expressed in the same way, but as a rate per day. The description of the results focuses on the emissions normalized per gram of soil carbon, whereas results per gram of dry soil are summarized in the tables and figures below. The abbreviations AL and PL refer to the active and permafrost layer, respectively.

3.4.1 Cumulative CH₄ Emissions

Cumulative CH₄ emissions (Figure 4) were significantly higher under anaerobic conditions than under aerobic conditions (t-test, uneq.var.t: P = 0.001). Under anaerobic conditions, they ranged from 0.16 ± 0.07 to 149.23 ± 35.79 $\mu\text{g CH}_4\text{-C gC}^{-1}$ and from 0.03 ± 0.01 to 176.95 ± 13.35 $\mu\text{g CH}_4\text{-C gsoil}^{-1}$, respectively, for all three analyzed cores and layers. When comparing the three cores, anaerobic emissions per gram of soil carbon were highest for P19. They were significantly higher in the active layer of P19 than in P24-AL (Tukey, P = 0.004) and P25-AL (Tukey, P < 0.001), as well as in the permafrost layer of P24 (Tukey, P = 0.015) and P25 (Tukey, P < 0.001). For P19, the emissions of the active layer sample were 149.23 ± 35.79 $\mu\text{g CH}_4\text{-C gC}^{-1}$, approximately two times higher than in the permafrost layer, although there was no significant difference (t-test, uneq.var.t: P = 0.077). Cumulative anaerobic emissions of P24 were similar for the active and permafrost layer, with 38.15 ± 2.88 and 34.66 ± 5.17 $\mu\text{g CH}_4\text{-C gC}^{-1}$, respectively, and thus were not significantly different (t-test, uneq.var.t: P = 0.464). The samples of P25 showed the lowest anaerobic CH₄ emissions with 0.62 ± 0.69 $\mu\text{g CH}_4\text{-C gC}^{-1}$ for the active layer and 0.16 ± 0.07 $\mu\text{g CH}_4\text{-C gC}^{-1}$ for the permafrost layer, respectively (no significance between layers, t-test, uneq.var.t: P = 0.447). Thus, in P19 and P25, emissions of the active layer sample were higher than in the permafrost layer, whereas P24 showed only little difference between the two segments.

When fluxes were expressed in per gram of dry soil (Figure 4), the pattern of cumulative C release changed as it considers differences in C quantity. Then, the active layer of P24 showed the highest emissions, with 176.95 ± 13.35 $\mu\text{g CH}_4\text{-C gsoil}^{-1}$, followed by the permafrost layer of P19 with 116.78 ± 24.47 $\mu\text{g CH}_4\text{-C gsoil}^{-1}$. P19-AL and P24-PL

released similar amounts of CH₄ per gram of dry soil and P25 again had the lowest emissions (Table 6). CH₄ emissions under aerobic conditions were very low since methane is mainly produced under anoxic conditions (Schuur et al., 2015; Angle et al., 2017). Therefore, they are not described in more detail but can be found in table 6.

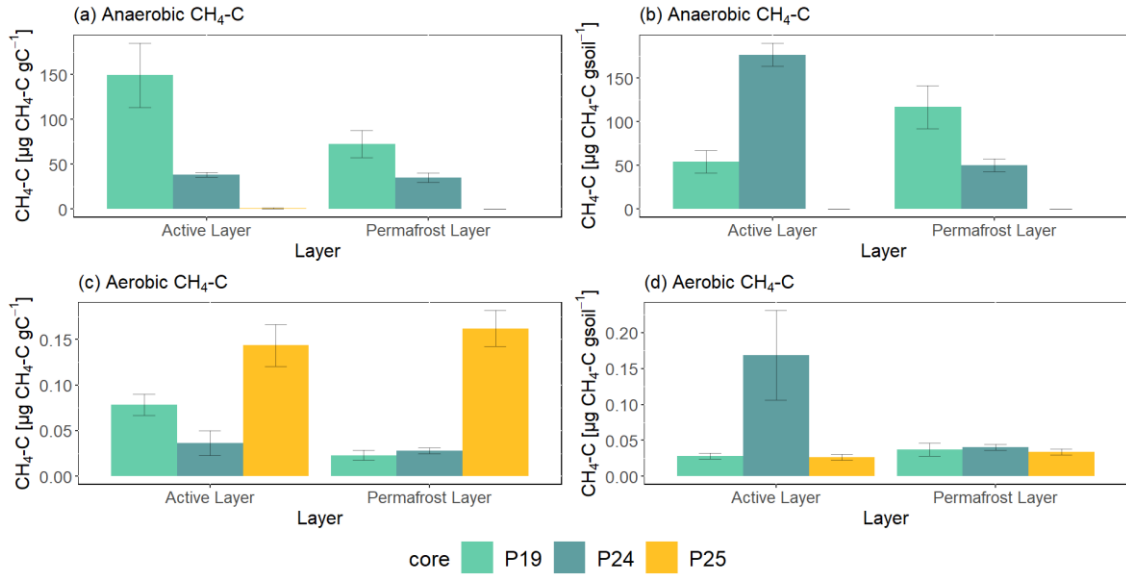


Figure 4 Cumulative CH₄ emissions during 68 days of incubation under anaerobic (a, b) and aerobic (c, d) conditions; units in µg CH₄-C gC⁻¹ (a,c) and µg CH₄-C gsoil⁻¹ (b,d); scale on y-axis is different between treatments and units; error bars represent the standard errors of three replicates (n=3).

3.4.2 Cumulative CO₂ Emissions

Cumulative CO₂ emissions under anaerobic conditions ranged from 43.39 ± 6.23 to 344.36 ± 101.69 µg CO₂-C gC⁻¹ and from 9.14 ± 1.31 to 417.33 ± 31.39 µg CO₂-C gsoil⁻¹ for all investigated cores and layers, respectively (Table 7). Under aerobic conditions, they were generally significantly higher (t-test, P = 0.006), mostly about two times, and varied from 82.92 ± 7.44 to 401.06 ± 13.93 µg CO₂-C gC⁻¹ and from 17.47 ± 1.57 to 856.12 ± 61.37 µg CO₂-C gsoil⁻¹, respectively. Significant differences between aerobic and anaerobic treatments were found for P19-PL (t-test, uneq.var.t: P = 0.002), P24-AL (t-test, uneq.var.t: P = 0.003), P24-PL (t-test, uneq.var.t: P = 0.003), P25-AL (t-test, uneq.var.t: P = 0.011), and P25-PL (t-test, P = 0.005), but not for P19-AL.

When comparing the emissions of the three cores under anaerobic conditions (Figure 5), CO₂ emissions per gram of soil carbon were highest for the samples of active and permafrost layer of P19, with 344.36 ± 101.69 µg CO₂-C gC⁻¹ and 130.33 ± 13.38 µg CO₂-C gC⁻¹, respectively. Significant differences were present when comparing P19-AL with P24-AL (Tukey, P = 0.012) and P25-AL (Tukey, P = 0.015) as well as P19-PL with P24-PL (Tukey, P = 0.015) and P25-PL (Tukey, P < 0.001). P24-AL and P25-AL were not significantly different from each other, but P24-PL and P25-PL (Tukey, P = 0.039).

Emissions of P24 were in a similar range, with $89.97 \pm 6.77 \mu\text{g CO}_2\text{-C gC}^{-1}$ in the active layer and $82.01 \pm 14.13 \mu\text{g CO}_2\text{-C gC}^{-1}$ in the permafrost layer. For P25, emissions in the active layer were $102.84 \pm 12.61 \mu\text{g CO}_2\text{-C gC}^{-1}$ and were lowest overall in the permafrost layer with $43.39 \pm 6.23 \mu\text{g CO}_2\text{-C gC}^{-1}$. Thus, in all three cores, CO_2 emissions of the active layer samples were higher than in the permafrost layer. However, significant differences between the two layers were present only in P25 (t-test, uneq.var.t.: $P = 0.010$).

When comparing the cores under aerobic conditions, P19 samples had the highest emissions overall with $401.06 \pm 13.93 \mu\text{g CO}_2\text{-C gC}^{-1}$ in the active layer and $311.45 \pm 23.77 \mu\text{g CO}_2\text{-C gC}^{-1}$ in the permafrost layer. Significant differences between cores were present in P19-AL and P24-AL (Tukey, $P < 0.001$) and P19-AL and P25-AL (Tukey, $P < 0.001$). Also, in the permafrost layer, all three cores were significantly different (Anova, $P < 0.001$). For samples of P24, emissions of the permafrost layer ($238.47 \pm 11.38 \mu\text{g CO}_2\text{-C gC}^{-1}$) were higher than those of the active layer ($184.56 \pm 13.23 \mu\text{g CO}_2\text{-C gC}^{-1}$) (t-test, uneq.var.t: $P = 0.013$). In P25, the active layer sample emitted $208.95 \pm 23.52 \mu\text{g CO}_2\text{-C gC}^{-1}$, which was more than twice as much as in the permafrost layer (t-test, uneq.var.t: $P = 0.011$). Thus, for P19 and P25, the total CO_2 emissions in the active layer were higher than in the permafrost layer, in contrast to P24. When fluxes were expressed per gram of dry soil, the pattern of cumulative C release was slightly different (Figure 5). As with methane emissions, the active layer sample of P24 had the highest CO_2 release both under anaerobic and aerobic conditions.

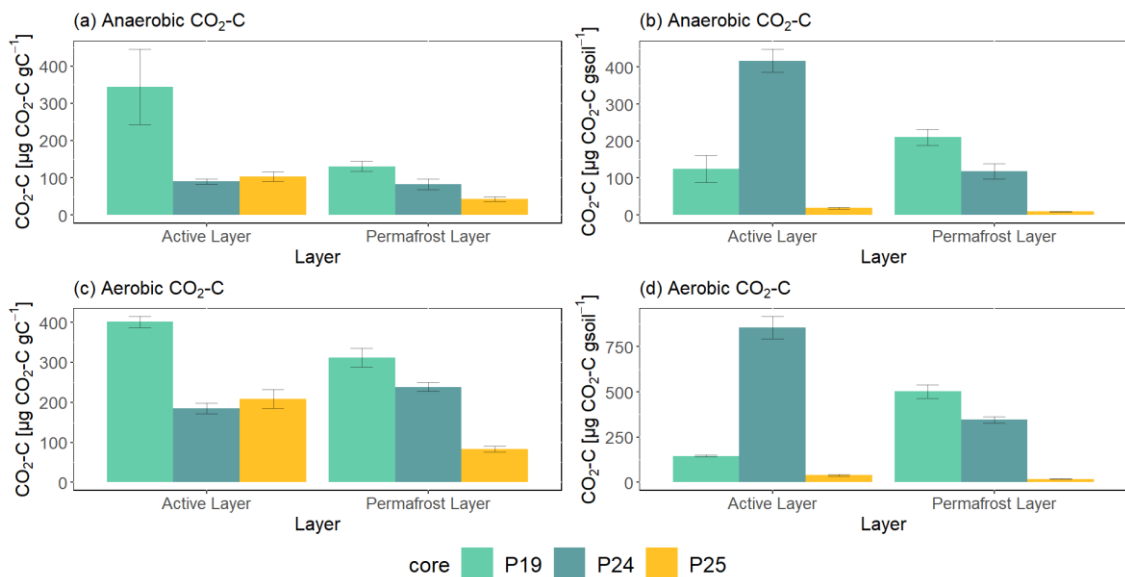


Figure 5 Cumulative CO_2 emissions during 68 days of incubation under anaerobic (a, b) and aerobic (c, d) conditions; units in $\mu\text{g CO}_2\text{-C gC}^{-1}$ (a,c) and $\mu\text{g CO}_2\text{-C gsoil}^{-1}$ (b,d); scale on y-axis is different between treatments and units; error bars represent the standard errors of three replicates ($n=3$).

Table 6 Cumulative CH₄ emissions and standard errors of replicates (n = 3) during 68 days of incubation under anaerobic and aerobic conditions, given in per gram of soil carbon ($\mu\text{g CH}_4\text{-C gC}^{-1}$) and per gram of dry soil ($\mu\text{g CH}_4\text{-C gsoil}^{-1}$).

Sample Name	CH ₄ Emissions anaerobic [$\mu\text{g CH}_4\text{-C gC}^{-1}$]	CH ₄ Emissions anaerobic [$\mu\text{g CH}_4\text{-C gsoil}^{-1}$]	CH ₄ Emissions aerobic [$\mu\text{g CH}_4\text{-C gC}^{-1}$]	CH ₄ Emissions aerobic [$\mu\text{g CH}_4\text{-C gsoil}^{-1}$]
P19 – active layer	149.23 ± 35.79	54.05 ± 12.96	0.08 ± 0.01	0.028 ± 0.004
P19 – permafrost layer	72.39 ± 15.17	116.78 ± 24.47	0.02 ± 0.01	0.037 ± 0.009
P24 – active layer	38.15 ± 2.88	176.95 ± 13.35	0.04 ± 0.01	0.169 ± 0.062
P24 – permafrost layer	34.66 ± 5.17	50.18 ± 7.49	0.03 ± 0.00	0.040 ± 0.004
P25 – active layer	0.62 ± 0.69	0.11 ± 0.13	0.14 ± 0.02	0.027 ± 0.004
P25 – permafrost layer	0.16 ± 0.07	0.03 ± 0.01	0.16 ± 0.02	0.034 ± 0.004

Table 7 Cumulative CO₂ emissions and standard errors of replicates (n = 3) during 68 days of incubation under anaerobic and aerobic conditions, given in per gram of soil carbon ($\mu\text{g CO}_2\text{-C gC}^{-1}$) and per gram of dry soil ($\mu\text{g CO}_2\text{-C gsoil}^{-1}$).

Sample Name	CO ₂ Emissions anaerobic [$\mu\text{g CO}_2\text{-C gC}^{-1}$]	CO ₂ Emissions anaerobic [$\mu\text{g CO}_2\text{-C gsoil}^{-1}$]	CO ₂ Emissions aerobic [$\mu\text{g CO}_2\text{-C gC}^{-1}$]	CO ₂ Emissions aerobic [$\mu\text{g CO}_2\text{-C gsoil}^{-1}$]
P19 – active layer	344.36 ± 101.69	124.73 ± 36.83	401.06 ± 13.93	145.26 ± 5.05
P19 – permafrost layer	130.33 ± 13.38	210.24 ± 21.59	311.45 ± 23.77	502.44 ± 38.34
P24 – active layer	89.97 ± 6.77	417.33 ± 31.39	184.56 ± 13.23	856.12 ± 61.37
P24 – permafrost layer	82.01 ± 14.13	118.72 ± 20.46	238.47 ± 11.38	345.24 ± 16.48
P25 – active layer	102.84 ± 12.61	19.01 ± 2.33	208.95 ± 23.52	38.63 ± 4.35
P25 – permafrost layer	43.39 ± 6.23	9.14 ± 1.31	82.92 ± 7.44	17.47 ± 1.57

3.4.3 Production Rate of Methane

The daily production rate during the 68-day incubation was calculated in $\mu\text{g CH}_4\text{-C gC}^{-1} \text{d}^{-1}$ and $\mu\text{g CO}_2\text{-C gC}^{-1} \text{d}^{-1}$, respectively, in order to understand how the gas production changed over time.

The production rates of CH_4 emissions (Figure 6) coincided with the cumulative emissions described above. They were higher under anaerobic conditions than under aerobic conditions, which were close to zero over the entire period. P19 showed the highest production rates. The active layer sample showed a fast increasing and high gas production during the first weeks, which then decreased from day 27 and increased again from day 47 until the end of the experiment. The permafrost layer sample remained in the lag phase until day 33, i.e., about half of the incubation period, and then increased continuously until day 61. The samples of the soil core P24 also showed a higher CH_4 production rate under anaerobic than under aerobic conditions. In the active layer sample, it increased in the first days and then fluctuated between $0.03\text{-}1.22 \mu\text{g CH}_4\text{-C gC}^{-1} \text{d}^{-1}$ throughout the incubation period. The permafrost layer sample, like in P19, was inactive until day 33 and then showed a continuous increase in production rate until day 68. The production rates of P25 were the lowest when comparing the cores. Both under aerobic and anaerobic conditions they were close to zero. Only the active layer sample had an increasing production rate in the anaerobic treatment at the end of the experiment.

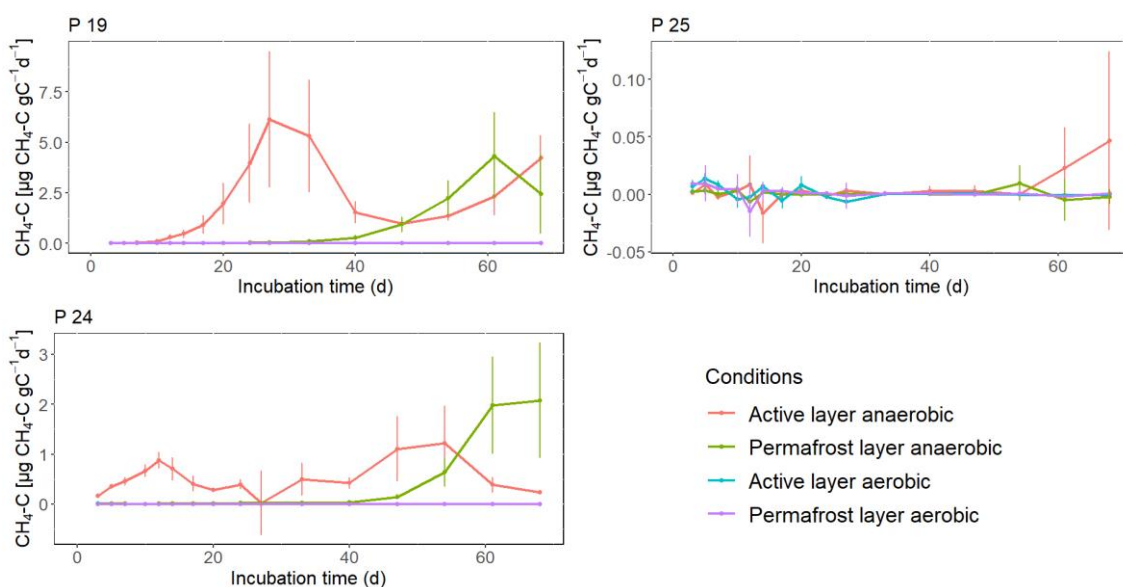


Figure 6 CH_4 production rate in $\text{CH}_4\text{-C gC}^{-1} \text{d}^{-1}$ over 68 days for samples from active and permafrost layer of P19, P24, and P25 under anaerobic and aerobic conditions; vertical lines represent the standard deviation resulting from the three replicates per core and layer.

3.4.4 Production Rate of Carbon Dioxide

The CO₂ production rates (Figure 7) showed a similar pattern in all samples. They started with high rates at the beginning of the incubation, which then rapidly decreased within two weeks to a low level. The production rates were consistent with the cumulative emissions described above. For P19, under anaerobic conditions, rates in the active layer sample were higher than in the permafrost layer for the first 40 days, then they decreased rapidly and remained in a low range. Under aerobic conditions, the production rates of the active and permafrost layer samples were initially similar, but from day 20 until the end of the incubation period, those from the active layer were higher. The permafrost layer sample under aerobic conditions had the lowest rate overall. Samples of P24 had lower production rates than those of P19 but show a similar pattern with initially high rates that rapidly decreased to a low steady state. Under aerobic conditions, gas production rates were higher than under anaerobic conditions. The differences between the active and permafrost layers of P24 were small in both treatments. The production rates of P25 were also lower than those of P19. The rates decreased to a low range from day 27 onwards. Overall, the active layer sample under aerobic conditions had a higher rate until day 68, whereas the permafrost layer under anaerobic conditions mostly had the lowest rate.

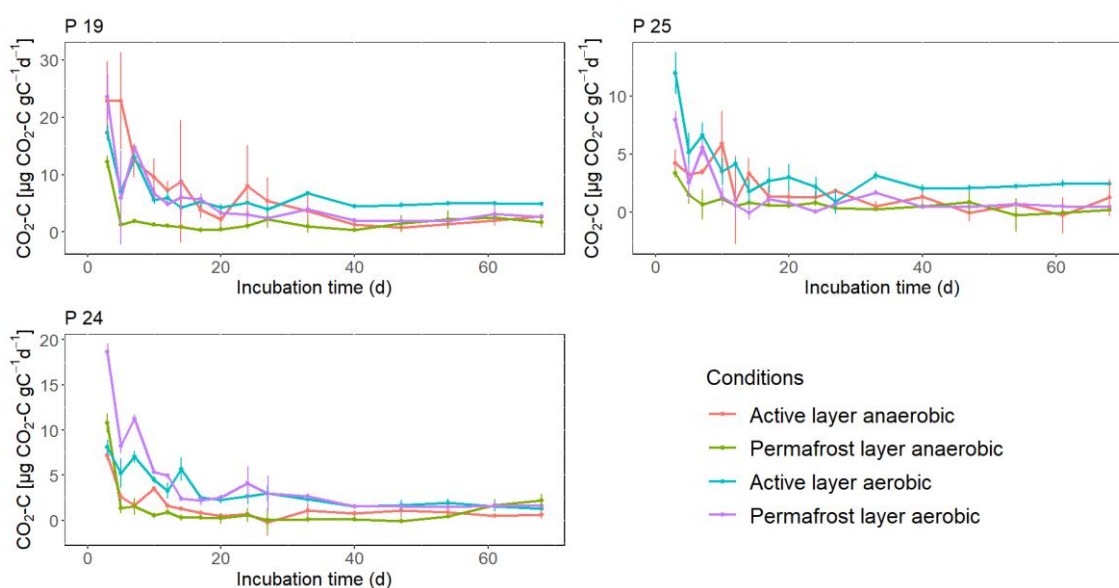


Figure 7 CO₂ production rate in CO₂-C gC⁻¹ d⁻¹ over 68 days for samples from active and permafrost layer of P19, P24, and P25 under anaerobic and aerobic conditions; vertical lines represent the standard deviation resulting from the three replicates per core and layer.

3.5 Relationship between Soil Characteristics and Gas Release

The relationships of the soil characteristics between each other as well as with the cumulative gas release were tested using the non-parametric Spearman correlation coefficient and are shown in table 8. Only the parameters of the cores P19, P24, and P25 were tested in more detail, as they were incubated and radiocarbon dated.

Correlations were tested for all three cores together to have a meaningful sample size. Significant correlations existed between the parameters water content and TOC ($\rho = 0.86$, $P < 0.001$), TOC and C/N ($\rho = 0.73$, $P = 0.003$), water content and sand fraction ($\rho = -0.89$, $P < 0.001$), water content and silt/clay fraction ($\rho = 0.89$, $P < 0.001$), TOC and sand fraction ($\rho = -0.89$, $P < 0.001$), TOC and silt/clay fraction ($\rho = 0.89$, $P < 0.001$), age and sand fraction ($\rho = -0.64$, $P = 0.044$), age and silt fraction ($\rho = 0.64$, $P = 0.044$), anaerobic emissions (per gram of dry soil) and TOC ($\rho = 0.89$, $P = 0.033$), aerobic emissions (per gram of dry soil) and TOC ($\rho = 0.94$, $P = 0.017$), aerobic emissions (per gram of dry soil) and sand fraction ($\rho = -0.99$, $P < 0.001$) as well as aerobic emissions (per gram of dry soil) and silt/clay fraction ($\rho = 0.99$, $P < 0.001$). Between all other parameters, such as between water content and C/N, emissions (per gram of soil carbon) and soil parameters as well as age and soil parameters there were no significant correlations (Table 8).

Figure 8 shows the soil characteristics and emissions in order to have a qualitative, visual comparison of the three in-depth analyzed, incubated cores. The correlations between grain size, water content, and TOC could be seen in all three cores. When the silt fraction increased or decreased, the water content and TOC also increased or decreased. This was also confirmed by the statistical analysis, which showed a statistically significant positive correlation between water content, TOC, and sand, silt, and clay fraction. The C/N had a similar trend to the above-mentioned parameters, but this could not be statistically tested as the TN was below detection limit in many layers. When comparing soil properties with radiocarbon ages and emissions (Figure 8 only shows the emissions per gram of soil carbon), the lack of correlation becomes apparent. However, it could be seen that P25 had a high sand content and a low TOC in most layers, and this was also reflected in the lower CH₄ and CO₂ emissions per gram of soil carbon, even though no significant correlation between these parameters could be determined.

Table 8 Matrix with correlation coefficient ρ , expressing intensity and direction of correlation between two parameters. Values with "*" indicate significant correlations ($P < 0.05$), values without "*" indicate no significant correlation between parameters.

	Total Organic Carbon	Water content	C/N ratio	Sand Fraction	Silt Fraction	Clay Fraction	Radiocarbon Age	Anaerobic Emissions (per g soil C)	Aerobic Emissions (per g soil C)	Anaerobic Emissions (per g dry soil)	Aerobic Emissions (per g dry soil)
Total Organic Carbon	-	-	-	-	-	-	-	-	-	-	-
Water Content	0.86*	-	-	-	-	-	-	-	-	-	-
C/N Ratio	0.73*	0.37	-	-	-	-	-	-	-	-	-
Sand Fraction	-0.89*	-0.89*	-0.12	-	-	-	-	-	-	-	-
Silt Fraction	0.89*	0.89*	0.12	-	-	-	-	-	-	-	-
Clay Fraction	0.88*	0.89*	0.11	-	-	-	-	-	-	-	-
Radiocarbon Age	0.18	0.33	-	-0.64*	0.64*	-0.60	-	-	-	-	-
Anaerobic Emissions (per g soil C)	0.54	-	-	-0.58	0.58	0.58	0.7	-	-	-	-
Aerobic Emissions (per g soil C)	0.14	-0.03	-	-0.20	0.20	0.20	0.4	-	-	-	-
Anaerobic Emissions (per g dry soil)	0.89*	-	-	-0.93	0.93	0.93	0.9	-	-	-	-
Aerobic Emissions (per g dry soil)	0.94*	0.94	-	-0.99*	0.99*	0.99*	0.9	-	-	-	-

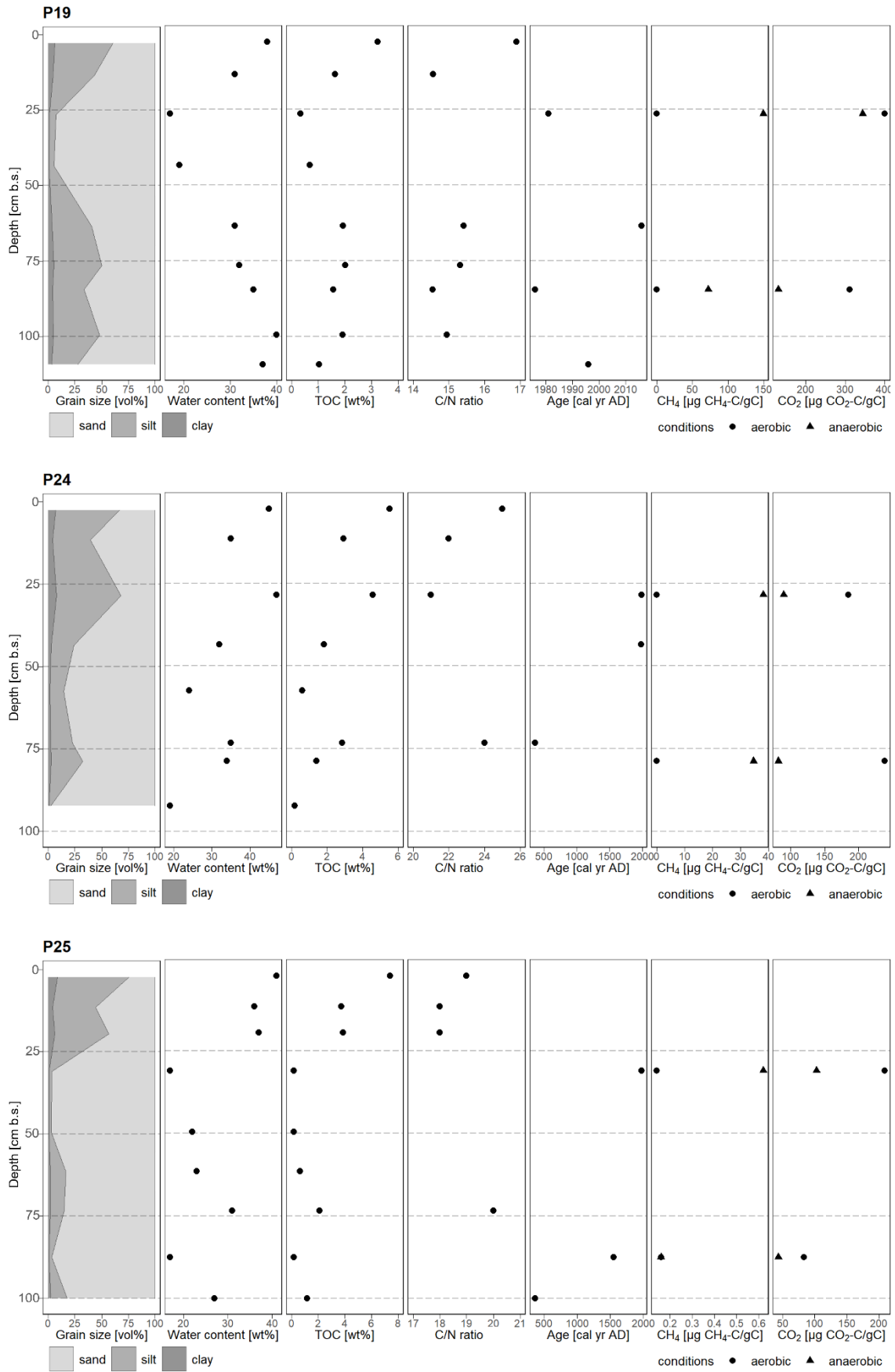


Figure 8 Summary of soil characteristics (grain size, water content, TOC, C/N ratio, radiocarbon age) and gas release (here shown in per gram of soil carbon) during aerobic and anaerobic incubation; note the different x-axis scaling between the cores.

4 Discussion

4.1 Carbon Characteristics of Active Floodplains

4.1.1 Hydrochemical Characterization

The pH value of all samples was in the neutral to slightly alkaline range (6.9-7.8), only in the deeper layers of P19 and P20 it was slightly lower than 7. Zubrzycki et al. (2013) determined similar pH values (6.5-7.3) for active floodplain soils on Samoylov, whereas Boike et al. (2013) determined lower, acidic pH values of 4.4-6.7 in the floodplains of Samoylov.

Conductivity ranged from 110 $\mu\text{S cm}^{-1}$ to 529 $\mu\text{S cm}^{-1}$ (without outliers). Juhls et al. (2020) studied water samples from the river surface in the center of the Olenekskaya Channel, the creek between Samoylov and Kurungnakh Island, which is responsible for early season flooding of the investigated active floodplains. They determined electrical conductivities from 99 to 490 $\mu\text{S cm}^{-1}$. This shows a high agreement with the electrical conductivities determined in the soils of the adjacent active floodplains and indicates that this is a potential source for the soil water in the analyzed cores.

4.1.2 Grain Size

Overall, the average sand fraction of all cores was high, as it was expected for active floodplain soils. However, the grain size distribution of the analyzed samples indicated a high heterogeneity in the soils of the active floodplains, as the sand, silt and clay fractions had a wide range (sand: 24.5-99.4%, silt: 0.5-66.9%, clay: 0-8.6%) and distribution varied from unimodal to polymodal and from very poorly sorted to well sorted. According to Boike et al. (2013), fluvial origin and continuous episodic reworking result in floodplain soils composed of stratified medium to fine sands and silts as well as layers of organic matter and peat. A peak in the sand fraction indicates that flowing water is the dominant transport process, whereas lower stream flow may lead to deposition of coarser silt. The mixture of unimodal, bimodal, trimodal, and polymodal distribution curves also indicates that the sediments may have been deposited not only by river, but also by alluvial and lacustrine processes (Fuchs et al., 2018). Overall, the mixed grain size signal reflects that the active floodplains are located in a very dynamic landscape, characterized by migrating river channels, spring flooding, and various depositional processes. Thawing permafrost and erosion processes due to climate change could increase discharge and sediment loads, which could impact the active floodplains at the river-permafrost interface (Bowden et al., 2008; Lamoureux et al., 2014; Lamoureux & Lafrenière, 2009).

4.1.3 Carbon and Nitrogen Contents

The organic carbon ranged from 0.11 to 7.39%, averaging $1.75 \pm 1.53\%$ for all soil samples. Overall, TOC varied between cores and with depth, indicating that active floodplain soils are very heterogeneous. The sample closest to the surface often had the highest carbon concentrations, which may be attributed to the presence of fresh organic matter due to vegetation (Knoblauch et al., 2013). But some cores also showed deeper organic-rich layers. This inhomogeneous distribution over depth indicates that carbon was stored by deltaic depositional processes rather than soil-forming processes (Fuchs et al., 2018). In comparison to previous studies, Zubrzycki et al. (2013) measured higher carbon contents in active floodplain soils on Samoylov, ranging from 0.13 to 27.71% and Laurent (2021) measured values between 0.17 to 5.98% in soil cores from the active floodplains of Kurungnakh Island, which is similar to the values found in this study. In general, it was expected that active, sparsely vegetated floodplains have lower carbon contents than older terraces in the Lena Delta. This cannot be confirmed overall. For example, Zubrzycki et al. (2013) found higher carbon contents of up to 42.46% for the Holocene terrace of Samoylov, whereas Knoblauch et al. (2013) found carbon contents only between 0.6% and 12.4% (sampling depth up to 25 m) in the Pleistocene terrace at Kurungnakh and the Holocene terrace at Samoylov, which is higher but in a similar range as the active floodplains. Thus, active floodplains may be more important than assumed, especially considering that not only soil-forming processes but also deltaic depositional processes are important for assessing carbon and nitrogen content in active floodplains. In addition, their large area within the Lena Delta makes them an important component of the total regional C stock.

Furthermore, total nitrogen and C/N ratios were determined. The total nitrogen contents were very low, ranging from <0.10% to 0.385%, and thus could be a limiting factor in the potential degradation of carbon. In many samples TN was below detection limit of 0.10%. Zubrzycki et al. (2013) analyzed similar values for TN ranging from 0.01 to 0.67% in active floodplains of Samoylov. For Holocene river terrace they found only slightly higher TN, ranging from 0.01 to 0.90%. The C/N ratio ranged between 14.37 and 24.75, which is consistent with findings in other studies. For example, Zubrzycki et al. (2013) determined an average C/N of 13 to 21 in the first meter of soil for Samoylovs active floodplains, and Knoblauch et al. (2013) reported a C/N from 10 to 25 for the Holocene and Pleistocene terraces on Samoylov and Kurungnakh Island.

4.1.4 Carbon and Nitrogen Stocks and Pools

SOC stocks ranged between 3.10 and 19.45 kg C m⁻² for the first meter of soil. As with carbon contents, SOC storages were also highly variable with depth. The overall average of all cores was 12.89 ± 6.02 kg C m⁻². About 40% of the organic carbon was stored in the first 30 cm, which represents the average depth of the seasonally thawed active layer during summer. According to estimates by Zubrzycki et al. (2013), the active floodplains occupy an area of 8830 km² in the Lena Delta. This results in a total carbon pool of 114 ± 53 Tg C for the first meter of soil in active floodplains of the Lena Delta.

Zubrzycki et al. (2013) also studied the carbon stocks in the Lena Delta. In their study, SOC stocks in the active floodplains ranged from 6.5 to 26.6 kg C m⁻² and averaged 13.6 ± 7.4 kg C m⁻², i.e., they are slightly higher but in a similar range. For the depth of 1 m, they estimated a total SOC pool of 120 ± 66 Tg C, which is higher than in this study. In the Ikpikpuk and Fish Creek River deltas in northern Alaska, Fuchs et al. (2018) determined mean SOC stocks of 16.5 kg C m⁻² (0-100 cm) for the sandbars, which is also slightly higher but comparable to this study. Siewert et al. (2016) reported mean SOC of 9.6 ± 6 kg C m⁻² for alluvial sediment and 17.7 ± 5.8 kg C m⁻² for the floodplains on Kurungnakh Island, which is also similar to the results in this study. Hugelius et al. (2011) found SOC stocks of 11.7 kg C m⁻² in the sediments of the Rgovaya River in northeastern European Russia, which is very close to the estimates of this study. In addition, Hugelius et al. (2014) reported revised estimates of 11.7 ± 7.6 kg C m⁻² for mean SOC stocks of the active floodplains in the Lena Delta.

Mean total nitrogen stocks ranged from 0.61 to 1.07 kg N m⁻² in the first meter of soil. The overall average of all soil profiles was 0.56 ± 0.38 kg N m⁻² of which about 42% was stored in the first 30 cm. When extrapolating the mean stock to the active floodplain area of 8830 km² within the Lena Delta, the total nitrogen pool is about 5 ± 3 Tg N (0-100 cm). Zubrzycki et al. (2013) reported a mean SN stock of 0.9 ± 0.40 kg N m⁻² (0-100 cm) for the active floodplains, which is higher than in this study. Consequently, they also estimated a higher total N pool at 7.7 ± 3.6 Tg N. Fuchs et al. (2018) determined mean soil N stocks between 0.5 and 1.78 kg N m⁻² (0-100 cm) for the Ikpikpuk and Fish Creek River deltas, which is slightly higher, probably because soil profiles of the wet tundra are included. Ping et al. (2011) measured mean soil N stocks along the Alaskan Beaufort Sea Coast about twice as high, at 1.2 ± 0.8 kg N m⁻² (0-100 cm).

Overall, the findings are consistent with the results of other studies. In general, active floodplains were expected to have lower mean SOC and SN stocks than other tundra environments. Siewert et al. (2016) assumes the following decreasing order for soil formation and SOC density: Pleistocene age non-degraded Ice Complex > Holocene aged terrace > degraded Ice Complex > recent floodplain > alluvial sediments. For comparison, Siewert et al. (2016) reported mean SOC stocks of $23.7 \pm 5.4 \text{ kg C m}^{-2}$ for the Holocene river terrace of Kurungnakh. Zubrzycki et al. (2013) determined an average of $29.5 \pm 10.5 \text{ kg C m}^{-2}$ in the Holocene river terrace of Samoylov, which is more than twice as high as in the active floodplains. However, they estimated a SOC pool of $121 \pm 43 \text{ Tg C}$ in the Holocene river terrace, which is comparable to the pool in the floodplains. This is because the soils in the active floodplains generally have a lower carbon density than soil in other tundra environments due to the larger fraction of sandy deposits and sand-dominated texture in soil layers (Fuchs et al., 2018), but overall occupy a larger area within the delta. This indicates that active floodplains should not be omitted when estimating C and N permafrost deposits. Due to ongoing permafrost thaw and resulting deepening of seasonally thawed active layer, carbon and nitrogen stocks in the perennially frozen ground, which is currently excluded from biogeochemical exchange with the atmosphere, may become increasingly available for decomposition processes, resulting in a C release to the atmosphere (Zubrzycki et al., 2013). The increasingly available nitrogen could also enhance the net primary production of vegetation, as nitrogen is one of the most important limiting factors (e.g., Shaver et al., 1986; Weintraub and Schimel 2003; Mack et al., 2004; Beermann et al., 2015).

This study indicates the importance of active floodplains as C and N permafrost deposits, although limited field data are available. For further robust and representative estimates, the strong spatial variability of active floodplain soils (inhomogeneous distribution of study sites and varying C and N contents within soil depth) must be considered in future data collection (Zubrzycki et al., 2013).

4.1.5 Radiocarbon Ages

The radiocarbon ages of all samples ranged from 360 ± 52 to 2016 ± 2 years AD and 0 ± 0 to 1590 ± 52.3 years BP, respectively, which indicates as expected very young material in the first meter of active floodplain soils. Fuchs et al. (2018) found similar values at comparable sites when studying the Ikpikpuk River delta in the Arctic coastal plain of northern Alaska. They determined ages up to 1115 ± 66 cal years BP for the first meter of soil. In comparison, other permafrost soils, such as the ice-rich and organic-rich

Yedoma ice complex deposits, which were formed by late Pleistocene deposition, are significantly older. Windirsch et al. (2020) found an age of up to 21,890 cal years BP for these in the first two meters of depth. The comparison with the Yedoma deposits illustrates how young the permafrost material of the active floodplains is and how rapid deposition and erosion likely occur and shape these permafrost soils.

Since not all layers of the core were radiocarbon dated, the radiocarbon dates only serve for a rough classification of the soil ages. For detailed results and age-depth relationships, the age must be dated over the entire depth. Nevertheless, in cores P24 and P25 a decrease of age with depth could be recognized, whereas in core P19 two age inversions occurred. Age inversions are not uncommon in such highly dynamic landscapes due to depositional and erosional processes during annual floods. Stanley et al. (2001) also mentioned problems with radiocarbon dating in modern river deltas as the sediment gets reworked, resulting in age inversions. However, the age inversions could also have been caused by contamination during field sampling or by picking material inappropriate for ^{14}C dating.

4.1.6 Accumulation Rates

Carbon accumulation rates ranged from $9.23 \text{ gC m}^{-2} \text{ yr}^{-1}$ to $320.62 \text{ gC m}^{-2} \text{ yr}^{-1}$ and sediment accumulation rates ranged between 0.44 mm yr^{-1} and 20.23 mm yr^{-1} . In core P19, the samples with age inversions had extremely high rates and were likely outliers. Conclusions about the accumulation rates over depth are therefore only plausible in P24 and P25. They had higher accumulation rates in the upper layers and lower accumulation rates in the deeper layers. In general, the range of rates over depth was large, indicating varying deposition and again highlighting the heterogeneity of these areas.

Fuchs et al. (2018) examined accumulation rates in two smaller river deltas in the Arctic coastal plain in Alaska. In the Ikpikpuk and Fish Creek River deltas, mean carbon accumulation rates ranged from 5.3 to $254.7 \text{ gC m}^{-2} \text{ yr}^{-1}$ and mean sediment accumulation rates ranged from 0.11 to 4.64 mm yr^{-1} . The rates are lower than in this study but vary less over depth. Similarly, the mean sediment accumulation rates (based on in situ measurements and include ice within sediment) reported by Jorgenson et al. (1998) for the Colville Delta in northern Alaska are generally lower with 2.6 mm yr^{-1} for active floodplain cover deposits, 0.4 mm yr^{-1} for delta abandoned floodplain cover deposits, and 1.3 mm yr^{-1} for delta inactive floodplain cover deposits. The higher rates in this study are likely due to the larger catchment area and higher river discharge in the Lena Delta, as this may influence sediment supply, transport, and deposition (Fuchs et al., 2018). But they can also be related to higher erosion in the other deltas. Since erosion rates are not

known, the calculated accumulation rates only allow us to draw conclusions about net accumulation. Overall, as expected due to regular flooding, deposition rates are high and show a wide range across the depth profile. The results underline that active floodplains are heterogeneous, dynamic and young permafrost environments characterized by sedimentation and erosion processes, where turnover of carbon is possible in a short time.

4.2 Potential Carbon Release from Active Floodplains

Climate models project a deepening of seasonally thawed active layer, altered moisture conditions and vegetation shifts in permafrost regions due to a changing climate, resulting in permafrost degradation, which makes carbon and nitrogen in deeper layers available for decomposition processes (Sazonova et al., 2004; Koven et al., 2011; Hinzman et al., 2005; Myers-Smith et al., 2011). Depending on whether oxic or saturated conditions develop, the primary decomposition products CO₂ and CH₄ vary, which in turn affects the feedback on climate (Treat et al., 2015).

Soils of active floodplains are periodically flooded during spring, temporarily favoring increased anaerobic conditions in addition to aerobic conditions. Climate change could cause not only warmer but also wetter soils in active floodplains, which in turn could lead to gas release under aerobic and anaerobic decomposition pathways (Knoblauch et al., 2013; Veremeeva et al., 2016). Therefore, the potential release of CH₄ and CO₂ under both conditions was investigated in this study. In addition, the differences between the upper, annually thawing active layer and the deeper, perennially frozen layer were examined.

4.2.1 Anaerobic vs. Aerobic Emissions

Cumulative methane emissions under anaerobic conditions showed a wide range for the analyzed cores and layers (0.16 ± 0.07 to $149.23 \pm 35.79 \mu\text{g CH}_4\text{-C gC}^{-1}$ and 0.03 ± 0.01 to $176.95 \pm 13.35 \mu\text{g CH}_4\text{-C gsoil}^{-1}$), which reflects the heterogeneity in the soils of the active floodplains already described in the soil characteristics. Under aerobic conditions, CH₄ production was very low, as methane is mainly produced under anoxic conditions (Schoor et al., 2015; Angle et al., 2017). Production rates of anaerobic CH₄ fluctuated in the active layer over the entire incubation period, whereas in the permafrost layer a lag phase of 30 days was observed, which may be related to a low abundance of active methanogen communities in the permafrost. Other studies (e.g., Laurent, 2021; Knoblauch et al., 2013; Walz et al., 2018; Holm et al., 2020; Bischoff et al., 2013; Wagner et al., 2007) also reported low initial production rates or long lag phases in permafrost

incubations, especially at lower incubation temperatures, as temperature strongly affects soil respiration rates in mineral permafrost soils (Mikan et al., 2002; Michaelson & Ping, 2003; Dutta et al., 2006). For example, Knoblauch et al. (2013) determined CH₄ productions in multi-year incubations of yedoma deposits in the Lena Delta (1200 d, 4 °C), which started after a significant delay of up to two years.

Cumulative CO₂ emissions under anaerobic conditions ranged from 43.39 ± 6.23 to 344.36 ± 101.69 $\mu\text{g CO}_2\text{-C gC}^{-1}$ and 9.14 ± 1.31 and 417.33 ± 31.39 $\mu\text{g CO}_2\text{-C gsoil}^{-1}$, respectively, for the analyzed cores and layers. Under aerobic conditions, they were higher, mostly two times. Accordingly, they varied between 82.92 ± 7.44 and 401.06 ± 13.93 $\mu\text{g CO}_2\text{-C gC}^{-1}$ and 17.47 ± 1.57 and 856.12 ± 61.37 $\mu\text{g CO}_2\text{-C gsoil}^{-1}$, respectively. Treat et al. (2014) reported in permafrost peat soil incubations at 20 °C, that cumulative CO₂ emissions under anaerobic conditions were about half of those under aerobic conditions, which is consistent with these results even though the soil type is different. The patterns of aerobic and anaerobic CO₂ production rates are similar per core (i.e., initially high rate that rapidly decreases and stays at a low level), which could mean that substrate quality of soil samples affects aerobic and anaerobic decomposition similarly (Lee et al., 2012). Lee et al. (2012) also reported similar patterns for CO₂ production rates under anaerobic and aerobic conditions and that aerobic rates were an order of magnitude higher than anaerobic rates. They also observed that aerobic CO₂ rates reached a quasi-steady-state at day 30, but under anaerobic conditions this was not until day 150. In contrast, in this study a steady state occurred after ~30 days in both treatments. The initial high CO₂ production rates indicate a large amount of labile carbon in the soil samples that is immediately available to the microbes (Dutta et al., 2006; Waldrop et al., 2010; Lee et al., 2012). Knoblauch et al. (2013) also observed a similar pattern in a multi-year incubation study with highest CO₂ respiration rates in both treatments in the first few weeks, which then also decreased rapidly until the end of the experiment.

Overall, total C emissions (CH₄ and CO₂) under aerobic conditions were up to twofold higher than under anaerobic conditions for five of six cores, both per gram of dry soil and per gram of soil carbon. Only for the active layer of P19 anaerobic emissions were slightly higher than aerobic emissions. This cannot be explained by soil properties but could be related to higher microbial abundance or to the landscape position, since this core is located on Kurungnakh, where soil layers could be influenced not only by deltaic processes but also by slope processes of the adjacent Yedoma.

In the studies by Knoblauch et al. (2013) and Lee et al. (2012), total emissions under aerobic conditions were even about a factor of six higher than under anaerobic conditions, which is much more than observed here.

4.2.2 Active vs. Permafrost Layer Emissions

Overall, total C emissions (CH_4 and CO_2) under anaerobic conditions were up to three times higher in the active layer than in the permafrost layer, except for P19 in per gram of dry soil, which may be due to the higher TOC in the permafrost layer. Treat et al. (2015) reported in a synthesis of anaerobic incubation studies that the maximum CH_4 production in the active layer was nearly four times higher than in the permafrost (per gram of soil carbon). Also, Laurent (2021) determined in an incubation of active floodplain samples at 20 °C significantly higher C release in the active than in the permafrost layer. In general, this difference could be related to the younger age of the active layer, which often stores more and higher quality organic matter, interacts with current vegetation, thaws annually and thus have intact microbial communities.

Cumulative C emissions (CH_4 and CO_2) under aerobic conditions were also higher in the active layer than in the permafrost layer, with exceptions for P24 in per gram of soil carbon and P19 in per gram of dry soil. For P24 no explanation could be found, but for P19 this is likely due to a lower TOC in active layer than in the permafrost layer.

The CO_2 production rate fluctuated for both layers in the first 20 days, but overall, there was a similar pattern for the active and permafrost layer over 68 days. The CH_4 production showed significant differences between the two layers. In the active layer, gas production started after a few days, fluctuated over the whole incubation period, and did not reach a steady until the end of incubation. Lee et al. (2012) reported in their incubation study that some CH_4 rates did not reach a steady state until day 300. In contrast, in the permafrost layer, methanogens did not become active before a lag phase of 30 days and also did not reach a steady production rate until the end of the experiment. This makes predictions for the further development difficult.

4.2.3 Relationship between Soil Characteristics and Carbon Release

Significant correlations were found between anaerobic and aerobic emissions per gram of dry soil and total organic carbon, as well as aerobic emissions per gram of dry soil and sand, silt and clay fraction. There were no significant correlations with any other soil properties and with emissions per gram of soil carbon. Overall, this indicates that soil texture and the amount of stored carbon affect the gas release. For example, the active

layer of P24 showed the highest anaerobic and aerobic CO₂ and CH₄ emissions per gram of dry soil and had the highest water content (47.0%) and TOC (4.566%). The permafrost layer of P19 had the second highest emissions per gram of dry soil and had the second highest water content (34.5%) and TOC (1.564%). Samples of soil core P25 had low water contents and the lowest TOC contents and were assigned to the soil texture "sand" and accordingly had low C emissions. Lee et al. (2012) also reported low production rates in mineral soils with low %C content. In general, soil moisture is an important factor in the decomposition process (Davidson & Janssens, 2006; Elberling et al., 2013) and mineralization of organic matter is favored the more labile and high-quality C and N compounds are present (Knoblauch et al., 2013; Lee et al., 2012; Aerts, 1997). Knoblauch et al. (2013) reported in their incubation study that initial aerobic and anaerobic CO₂ production rates correlated most strongly with TOC and TN.

P19 showed the highest emissions per gram of dry soil when comparing the permafrost layers of the cores, which could not only be related to moisture and TOC but could also be due to the slightly acidic pH of this sample, as the optimum for methanogenic bacteria is between acidic and neutral (Valentine et al., 1994; Bergman et al., 1998; Williams & Crawford, 1985; Dunfield et al., 1993).

However, not all findings could be explained with soil properties. For example, the active layer of P19 and the permafrost layer of P24 had approximately the same total anaerobic CO₂ and CH₄ emissions per gram of dry soil, although P24-PL had a four times higher TOC. The lack of correlation between emissions and soil properties could be due to the presence or absence of intact methanogenic communities. This was also indicated by the aerobic CO₂ emissions, as these were higher in P24-PL than in P19-AL. Laurent (2021) was able to explain high CH₄ emissions in the active floodplains with high copies number of methanogens in her incubation study.

The comparison of emissions per gram of soil carbon and per gram of dry soil was also interesting. Per gram of dry soil, CO₂ and CH₄ emissions were generally highest in P24-AL. However, when emissions were expressed per gram of soil carbon, emissions in P19-AL were highest. This means that although P24 released more carbon per gram of dry soil, the carbon in P19 was more bioavailable to microbes and more easily decomposable. Therefore, not only the amount of carbon stored but also its quality had an important role in C turnover. In addition, P19 had the youngest layers, which could mean that recently deposited, modern carbon was highly available to the microbes, whereas decomposition in P24 took longer due to the poorer carbon quality.

These experimental laboratory data gave a first indication of the potential C release in soils of the active floodplains. However, the trajectory of these permafrost areas is determined by many other mechanisms at ecosystem level (Knoblauch et al., 2013). To understand those, not only soil environmental conditions (temperature, relative water table position) and soil properties (organic matter quantity and quality, pH, soil type), but also permafrost history (deposition of organic matter under different past climatic conditions) and landscape-level factors (e.g., vegetation type and dynamics, landscape position) must be considered to assess the potential magnitude, timing, and form of C release in permafrost soils (Treat et al., 2014; Treat et al., 2015). Analysis of microbial community composition also need to be considered, as shown in the study by Laurent (2021) and others. Also, further in situ measurements are needed to consider processes such as oxidation of CH₄ in aerobic surface layers, alternative transport pathways, plant-soil interactions and the complete balance between uptake and release (Knoblauch et al., 2008; Kip et al., 2010; Treat et al., 2015). In addition, it is recommended to extend the incubation period from 68 days to the real duration of the growing season. The incubation temperature of 20 °C does not represent real conditions but was chosen since a long lag-phase was expected at 4 °C within 70 days (see Laurent, 2021). In addition, it would be important to incubate all layers of the depth profile and not only one sample per active and permafrost layer.

5 Conclusion

This is one of the first studies systematically analyzing carbon stocks, carbon accumulation and carbon release from active floodplains in the Lena River Delta. The study highlights the important role of those permafrost environments as carbon storages and provides valuable information for future studies on active floodplains in Arctic river deltas.

The analysis showed that, the mean SOC stock is $12.89 \pm 6.02 \text{ kg C m}^{-2}$ and the SOC pool for the active floodplains in the Lena Delta was estimated to $\sim 114 \pm 53 \text{ Tg C}$, which is comparable to the SOC pool of the Holocene river terrace estimated in other studies. This is explained by the large area that active floodplains occupy, even though they have a lower carbon density compared to soils of other Lena Delta terraces. Therefore, the active deltaic floodplains are significant permafrost carbon pools, which could become vulnerable to microbial decomposition, leading to a release of CH_4 and CO_2 , and which have not been in detail considered in the permafrost carbon climate feedback so far. Overall, the carbon stocks showed large differences between the vegetated and non-vegetated sites and varied with depth, including deeper organic-rich layers, and indicating that these are permafrost environments characterized not only by classical soil forming processes but by deltaic, riverine, and fluvial processes as well. This was also confirmed by the comparatively young radiocarbon ages up to 1 m in depth and the accumulation rates varying with depth. Climate change may intensify these different processes, particularly thawing and erosion, but also river discharge, which might result in a higher sediment input. This leads to the question whether these active floodplains become larger carbon sinks in future or whether this sink potential is offset by thawing permafrost and increasing CH_4 and CO_2 emissions. Future studies should investigate in more detail this carbon sink or source potential of active floodplains in permafrost dominated Arctic deltas, as these differ from other permafrost environments, where carbon inputs are primarily derived from vegetation.

The incubation analysis showed that the active floodplains potentially release CH_4 and CO_2 during thawing, although in lower amounts than other permafrost soils. Correlations were found between emissions (per gram of dry soil) and total organic carbon, and soil texture, indicating that high gas production could also occur in deeper organic-rich layers. Also, the comparison of emissions per gram of dry soil and per gram of soil carbon indicated that not only carbon quantity but also its quality has an important impact on decomposition. Emissions under aerobic conditions were mostly two times higher than

under anaerobic conditions. Changing soil hydrology due to climate change could alter this by favoring anaerobic conditions, which would lead to higher CH₄ emissions, indicating the need for further studies on C sink or C source potential of active floodplains.

Due to its comprehensive study design that included the investigation of carbon stocks, radiocarbon ages, accumulation rates as well as an incubation experiment of three soil cores, this study is an important basis for further studies to estimate the carbon stocks and carbon release potential of active floodplains in Arctic river deltas, as they occupy a large area in the deltas and are highly dynamic due to periodic erosion and sedimentation. Despite relatively homogeneous vegetation, this investigation of soil characteristics showed a high spatial variability with depth in terms of carbon contents, soil texture, accumulation rates, and emissions. This indicates the importance of analyzing the soil cores according to its facies horizons and performing incubations over the entire depth profile to characterize these environments.

Acknowledgement

This thesis was carried out in the FluxWIN research group at the Alfred Wegener Institute, Helmholtz Centre for Polar and Marine Research. The soil samples were collected during the Russian-German Lena Expedition in 2018 as part of the BMBF funded Kohlenstoff im Permafrost (KoPf) project. Laboratory analyses were performed at the Alfred Wegener Institute and the German Research Centre for Geosciences in Potsdam. I would like to thank the entire FluxWIN research group, led by Claire Treat, for making this thesis possible, providing the samples and laboratory facilities, as well as the supervision and support.

References

- Aerts, R. (1997). Climate, Leaf Litter Chemistry and Leaf Litter Decomposition in Terrestrial Ecosystems: A Triangular Relationship. *Oikos*, 79(3), 439–449. <https://doi.org/10.2307/3546886>
- Angle, J. C., Morin, T. H., Solden, L. M., Narrowe, A. B., Smith, G. J., Borton, M. A., Rey-Sanchez, C., Daly, R. A., Mirfenderesgi, G., Hoyt, D. W., Riley, W. J., Miller, C. S., Bohrer, G., & Wrighton, K. C. (2017). Methanogenesis in oxygenated soils is a substantial fraction of wetland methane emissions. *Nature Communications*, 8(1), 1567. <https://doi.org/10.1038/s41467-017-01753-4>
- Are, F., & Reimnitz, E. (2000). An overview of the Lena River Delta setting: Geology, tectonics, geomorphology, and hydrology. *Journal of Coastal Research*, 16, 1083–1093.
- Beermann, F., Teltewskoi, A., Fiencke, C., Pfeiffer, E.-M., & Kutzbach, L. (2015). Stoichiometric analysis of nutrient availability (N, P, K) within soils of polygonal tundra. *Biogeochemistry*, 122(2), 211–227. <https://doi.org/10.1007/s10533-014-0037-4>
- Bergman, I., Svensson, B. H., & Nilsson, M. (1998). Regulation of methane production in a Swedish acid mire by pH, temperature and substrate. *Soil Biology and Biochemistry* (United Kingdom). https://scholar.google.com/scholar_lookup?title=Regulation+of+methane+production+in+a+Swedish+acid+mire+by+pH%2C+temperature+and+substrate&author=Bergman%2C+I.&publication_year=1998
- Bischoff, J., Mangelsdorf, K., Gattinger, A., Schloter, M., Kurchatova, A. N., Herzsuh, U., & Wagner, D. (2013). Response of methanogenic archaea to Late Pleistocene and Holocene climate changes in the Siberian Arctic. *Global Biogeochemical Cycles*, 27(2), 305–317. <https://doi.org/10.1029/2011GB004238>
- Blott, S. J., & Pye, K. (2001). GRADISTAT: A grain size distribution and statistics package for the analysis of unconsolidated sediments. *Earth Surface Processes and Landforms*, 26(11), 1237–1248. <https://doi.org/10.1002/esp.261>
- Bowden, W. B., Gooseff, M. N., Balsler, A., Green, A., Peterson, B. J., & Bradford, J. (2008). Sediment and nutrient delivery from thermokarst features in the foothills of the North Slope, Alaska: Potential impacts on headwater stream ecosystems. *Journal of Geophysical Research: Biogeosciences*, 113(G2). <https://doi.org/10.1029/2007JG000470>
- Christensen, T. R., Johansson, T., Åkerman, H. J., Mastepanov, M., Malmer, N., Friborg, T., Crill, P., & Svensson, B. H. (2004). Thawing sub-arctic permafrost: Effects on vegetation and methane emissions. *Geophysical Research Letters*, 31(4). <https://doi.org/10.1029/2003GL018680>
- Davidson, E. A., & Janssens, I. A. (2006). Temperature sensitivity of soil carbon decomposition and feedbacks to climate change. *Nature*, 440(7081), 165–173. <https://doi.org/10.1038/nature04514>
- Dunfield, P., Knowles, R., Dumont, R., & Moore, T. R. (1993). Methane production and consumption in temperate and subarctic peat soils: Response to temperature and pH. *Soil Biology and Biochemistry*, 25(3), 321–326. [https://doi.org/10.1016/0038-0717\(93\)90130-4](https://doi.org/10.1016/0038-0717(93)90130-4)
- Dutta, K., Schuur, E. a. G., Neff, J. C., & Zimov, S. A. (2006). Potential carbon release from permafrost soils of Northeastern Siberia. *Global Change Biology*, 12(12), 2336–2351. <https://doi.org/10.1111/j.1365-2486.2006.01259.x>
- Elberling, B., Michelsen, A., Schädel, C., Schuur, E. A. G., Christiansen, H. H., Berg, L., Tamstorf, M. P., & Sigsgaard, C. (2013). Long-term CO₂ production following

- permafrost thaw. *Nature Climate Change*, 3(10), 890–894. <https://doi.org/10.1038/nclimate1955>
- Everdingen, van R.O. (1998). Multi-Language Glossary of Permafrost and Related Ground-Ice Terms. National Snow and Ice Data Center, Boulder, CO.
- Folk, R. L., & Ward, W. C. (1957). Brazos River bar [Texas]; a study in the significance of grain size parameters. *Journal of Sedimentary Research*, 27(1), 3–26. <https://doi.org/10.1306/74D70646-2B21-11D7-8648000102C1865D>
- Fuchs, M. (2019). Soil organic carbon and nitrogen pools in thermokarst-affected permafrost terrain [Phd, Universität Potsdam]. p. 109. In *EPIC3*. <https://epic.awi.de/id/eprint/51514/>
- Fuchs, M., Grosse, G., Jones, B. M., Strauss, J., Baughman, C. A., & Walker, D. A. (2018). Sedimentary and geochemical characteristics of two small permafrost-dominated Arctic river deltas in northern Alaska. *Arktos*, 4(1), 1–18. <https://doi.org/10.1007/s41063-018-0056-9>
- Grigoriev, M. (1993). Cryomorphogenesis in the Lena Delta (in Russian). Permafrost Institute Press, Yakutsk, 176 pp.
- Grosse, G., Harden, J., Turetsky, M., McGuire, A., Camill, P., Tarnocai, C., Frohling, S., Schuur, E., Jorgenson, T., Marchenko, S., Romanovsky, V., Wickland, K., French, N., Waldrop, M., Bourgeau-Chavez, L., & Striegl, R. (2011). Vulnerability of high-latitude soil organic carbon in North America to disturbance. *J. Geophys. Res.*, 116, G00K06. <https://doi.org/10.1029/2010jg001507>
- Harden, J. W., Mark, R. K., Sundquist, E. T., & Stallard, R. F. (1992). Dynamics of soil carbon during deglaciation of the Laurentide ice sheet. *Science (New York, N.Y.)*, 258(5090), 1921–1924. <https://doi.org/10.1126/science.258.5090.1921>
- Hinzman, L. D., Bettez, N. D., Bolton, W. R., Chapin, F. S., Dyurgerov, M. B., Fastie, C. L., Griffith, B., Hollister, R. D., Hope, A., Huntington, H. P., Jensen, A. M., Jia, G. J., Jorgenson, T., Kane, D. L., Klein, D. R., Kofinas, G., Lynch, A. H., Lloyd, A. H., McGuire, A. D., ... Yoshikawa, K. (2005). Evidence and implications of recent climate change in northern Alaska and other arctic regions. *Climatic Change*. 72: 251–298. <http://www.fs.usda.gov/treearch/pubs/25527>
- Hobbie, S. (2000). Interactions between Litter Lignin and Nitrogen Lignin and Soil Nitrogen Availability during Leaf Litter Decomposition in a Hawaiian Montane Forest. *Ecosystems*, 3, 484–494. <https://doi.org/10.1007/s100210000042>
- Holm, S., Walz, J., Horn, F., Yang, S., Grigoriev, M. N., Wagner, D., Knoblauch, C., & Liebner, S. (2020). Methanogenic response to long-term permafrost thaw is determined by paleoenvironment. *FEMS Microbiology Ecology*, 96(3), fiaa021. <https://doi.org/10.1093/femsec/fiaa021>
- Hugelius, G., Strauss, J., Zubrzycki, S., Harden, J. W., Schuur, E. A. G., Ping, C.-L., Schirmer, L., Grosse, G., Michaelson, G. J., Koven, C. D., O'Donnell, J. A., Elberling, B., Mishra, U., Camill, P., Yu, Z., Palmtag, J., & Kuhry, P. (2014). Estimated stocks of circumpolar permafrost carbon with quantified uncertainty ranges and identified data gaps. *Biogeosciences*, 11(23), 6573–6593. <https://doi.org/10.5194/bg-11-6573-2014>
- Hugelius, G., Virtanen, T., Kaverin, D., Pastukhov, A., Rivkin, F., Marchenko, S., Romanovsky, V., & Kuhry, P. (2011). High-resolution mapping of ecosystem carbon storage and potential effects of permafrost thaw in periglacial terrain, European Russian Arctic. *Journal of Geophysical Research*, 116. <https://doi.org/10.1029/2010JG001606>
- IPCC, 2022: Climate Change 2022: Impacts, Adaptation, and Vulnerability. Contribution of Working Group II to the Sixth Assessment Report of the Intergovernmental Panel on Climate Change [H.-O. Pörtner, D.C. Roberts, M. Tignor, E.S. Poloczanska, K.

- Mintenbeck, A. Alegría, M. Craig, S. Langsdorf, S. Löschke, V. Möller, A. Okem, B. Rama (eds.]. Cambridge University Press. In Press.
- Johansson, T., Malmer, N., Crill, P. M., Friborg, T., Åkerman, J. H., Mastepanov, M., & Christensen, T. R. (2006). Decadal vegetation changes in a northern peatland, greenhouse gas fluxes and net radiative forcing: DECADEAL CHANGES OF CARBON FLUX AND FORCING. *Global Change Biology*, *12*(12), 2352–2369. <https://doi.org/10.1111/j.1365-2486.2006.01267.x>
- Jorgenson, M.T., Shur, Y.L., Walker, H.J. (1998). Evolution of a permafrost-dominated landscape on the Colville River Delta, Northern Alaska. In: Lewkowicz AG, Allard M (eds) Proceedings of the seventh international conference on permafrost, Yellowknife, Canada, 1998. Collection Nordica, Yellowknife, pp 523–529.
- Juhls, B., Stedmon, C. A., Morgenstern, A., Meyer, H., Hölemann, J., Heim, B., Povazhnyi, V., & Overduin, P. P. (2020). Identifying Drivers of Seasonality in Lena River Biogeochemistry and Dissolved Organic Matter Fluxes. *Frontiers in Environmental Science*, *8*, 53. <https://doi.org/10.3389/fenvs.2020.00053>
- Kip, N., van Winden, J. F., Pan, Y., Bodrossy, L., Reichart, G.-J., Smolders, A. J. P., Jetten, M. S. M., Damsté, J. S. S., & Op den Camp, H. J. M. (2010). Global prevalence of methane oxidation by symbiotic bacteria in peat-moss ecosystems. *Nature Geoscience*, *3*(9), 617–621. <https://doi.org/10.1038/ngeo939>
- Knoblauch, C., Beer, C., Sosnin, A., Wagner, D., & Pfeiffer, E.-M. (2013). Predicting long-term carbon mineralization and trace gas production from thawing permafrost of Northeast Siberia. *Global Change Biology*, *19*(4), 1160–1172. <https://doi.org/10.1111/gcb.12116>
- Knoblauch, C., Zimmermann, U., Blumenberg, M., Michaelis, W., & Pfeiffer, E.-M. (2008). Methane turnover and temperature response of methane-oxidizing bacteria in permafrost-affected soils of northeast Siberia. *Soil Biology and Biochemistry*, *40*, 3004–3013. <https://doi.org/10.1016/j.soilbio.2008.08.020>
- Köchy, M., Hiederer, R., & Freibauer, A. (2015). Global distribution of soil organic carbon – Part 1: Masses and frequency distributions of SOC stocks for the tropics, permafrost regions, wetlands, and the world. *SOIL*, *1*(1), 351–365. <https://doi.org/10.5194/soil-1-351-2015>
- Koven, C. D., Ringeval, B., Friedlingstein, P., Ciais, P., Cadule, P., Khvorostyanov, D., Krinner, G., & Tarnocai, C. (2011). Permafrost carbon-climate feedbacks accelerate global warming. *Proceedings of the National Academy of Sciences*, *108*(36), 14769–14774. <https://doi.org/10.1073/pnas.1103910108>
- Kruse, S., Bolshiyarov, D., Grigoriev, M., Morgenstern, A., Pestryakova, L., Tsibizov, L., & Udke, A. (2019). Reports on Polar and Marine Research: Russian-German Cooperation: Expeditions to Siberia in 2018. Alfred Wegener Institute, Helmholtz Centre for Polar and Marine Research Bremerhaven.
- Lamoureux, S.F., Lafrenière, M.J., Favaro, E.A. (2014). Erosion dynamics following localized permafrost slope disturbances. *Geophys Res Lett* *41*(15):5499–5505. <https://doi.org/10.1002/2014GL060677>
- Lamoureux, S. F., & Lafrenière, M. J. (2009). Fluvial Impact of Extensive Active Layer Detachments, Cape Bounty, Melville Island, Canada. *Arctic, Antarctic, and Alpine Research*, *41*(1), 59–68. <https://doi.org/10.1657/1523-0430-41.1.59>
- Landgraf, N. (2020). Soil nutrients and their connection to arctic vegetation communities in the permafrost landscape of the central Lena Delta. Bachelor Thesis. University of Leipzig.
- Laurent, M. (2021). Links between greenhouse gas emissions and microbes shift during short-term permafrost thaw under anaerobic conditions. Master Thesis. Ecole Nationale Supérieure d'Environnement, des Géorressources et du Développement durable -Bordeaux INP.

- Lee, H., Schuur, E. A. G., Inglett, K. S., Lavoie, M., & Chanton, J. P. (2012). The rate of permafrost carbon release under aerobic and anaerobic conditions and its potential effects on climate. *Global Change Biology*, 18(2), 515–527. <https://doi.org/10.1111/j.1365-2486.2011.02519.x>
- Mack, M.C., Schuur, E.A.G., Bret-Harte, M.S., Shaver, G.R., Chapin, I. (2004). Ecosystem carbon storage in arctic tundra reduced by long-term nutrient fertilization. *Nature* 431:440. <https://doi.org/10.1038/nature02887>
- McGuire, A. D., Anderson, L. G., Christensen, T. R., Dallimore, S., Guo, L., Hayes, D. J., Heimann, M., Lorenson, T. D., Macdonald, R. W., & Roulet, N. (2009). Sensitivity of the carbon cycle in the Arctic to climate change. *Ecological Monographs*, 79(4), 523–555. <https://doi.org/10.1890/08-2025.1>
- Meijboom, F., Noordwijk, van M. (1991). Rhizon soil solution samplers as artificial roots. In: Kutschera L, Huebl E, Lichtenegger E, Persson H, Sobotnik M (eds), Root ecology and its practical application. 3 ISRR Symposium Verein für Wurzelforschung, A-9020 Klagenfurt, Austria, pp 793–795.
- Michaelson, G. J., Ping, C. L., & Kimble, J. M. (1996). Carbon Storage and Distribution in Tundra Soils of Arctic Alaska, U.S.A. *Arctic and Alpine Research*, 28(4), 414–424. <https://doi.org/10.2307/1551852>
- Michaelson, G., & Ping, C.-L. (2003). Soil Organic Carbon and CO₂ Respiration at Subzero Temperature in Soils of Arctic Alaska. *Journal of Geophysical Research*, 108. <https://doi.org/10.1029/2001JD000920>
- Mikan, C., Schimel, J., & Doyle, A. (2002). Temperature Controls of Microbial Respiration in Arctic Tundra Soils Above and Below Freezing. *Soil Biology and Biochemistry*, 34, 1785–1795. [https://doi.org/10.1016/S0038-0717\(02\)00168-2](https://doi.org/10.1016/S0038-0717(02)00168-2)
- Mollenhauer, G., Grotheer, H., Gentz, T., Bonk, E., & Hefter, J. (2021). Standard operation procedures and performance of the MICADAS radiocarbon laboratory at Alfred Wegener Institute (AWI), Germany. *Nuclear Instruments and Methods in Physics Research Section B: Beam Interactions with Materials and Atoms*, 496, 45–51. <https://doi.org/10.1016/j.nimb.2021.03.016>
- Morgenstern, A., Grosse, G., & Schirrmeister, L. (o. J.). *Genetic, Morphological, and Statistical Characterization of Lakes in the Permafrost-Dominated Lena Delta*. 6.
- Myers-Smith, I. H., Forbes, B. C., Wilmking, M., Hallinger, M., Lantz, T., Blok, D., Tape, K. D., Macias-Fauria, M., Sass-Klaassen, U., Lévesque, E., Boudreau, S., Ropars, P., Hermanutz, L., Trant, A., Collier, L. S., Weijers, S., Rozema, J., Rayback, S. A., Schmidt, N. M., ... Hik, D. S. (2011). Shrub expansion in tundra ecosystems: Dynamics, impacts and research priorities. *Environmental Research Letters*, 6(4), 045509. <https://doi.org/10.1088/1748-9326/6/4/045509>
- Natali, S. M., Schuur, E. a. G., Webb, E., Pries, C. E. H., & Crummer, K. G. (2014). Permafrost degradation stimulates carbon loss from experimentally warmed tundra. *Ecology and Society*, 95(3), 602–608.
- Oblogov, G. E., Vasiliev, A. A., Streletskaia, I. D., Zadorozhnaya, N. A., Kuznetsova, A. O., Kanevskiy, M. Z., & Semenov, P. B. (2020). Methane Content and Emission in the Permafrost Landscapes of Western Yamal, Russian Arctic. *Geosciences*, 10(10), 412. <https://doi.org/10.3390/geosciences10100412>
- O'Donnell, J., Jorgenson, T., Harden, J., McGuire, A., Kanevskiy, M., & Wickland, K. (2012). The Effects of Permafrost Thaw on Soil Hydrologic, Thermal, and Carbon Dynamics in an Alaskan Peatland. *Ecosystems*, 15. <https://doi.org/10.1007/s10021-011-9504-0>
- Ping, C.-L., Michaelson, G. J., Guo, L., Jorgenson, M. T., Kanevskiy, M., Shur, Y., Dou, F., & Liang, J. (2011). Soil carbon and material fluxes across the eroding Alaska Beaufort Sea coastline. *Journal of Geophysical Research: Biogeosciences*, 116(G2). <https://doi.org/10.1029/2010JG001588>

- Reimer, P.J., Brown, T.A., & Reimer, R.W. (2004). Discussion: Reporting and Calibration of Post-Bomb¹⁴C Data. *Radiocarbon*, 46, p 1299-1304.
- Reimer, R.W., & Reimer, P.J. (2022). CALIBomb [WWW program] at <http://calib.org> accessed 2022-1-24.
- Robertson, G. P., Coleman, D. C., Bledsoe, C. S., & Sollins, P. (Hrsg.). (1999). *Standard Soil Methods for Long-Term Ecological Research*. Oxford University Press.
- Romanovskii, N., & Hubberten, H.W. (2001). Results of permafrost modelling of the lowlands and shelf of the Laptev Sea Region, Russia. *Permafrost and Periglacial Processes*, 12, 191–202. <https://doi.org/10.1002/ppp.387>
- Romanovsky, V. E., Drozdov, D. S., Oberman, N. G., Malkova, G. V., Kholodov, A. L., Marchenko, S. S., Moskalenko, N. G., Sergeev, D. O., Ukraintseva, N. G., Abramov, A. A., Gilichinsky, D. A., & Vasiliev, A. A. (2010). Thermal state of permafrost in Russia. *Permafrost and Periglacial Processes*, 21(2), 136–155. <https://doi.org/10.1002/ppp.683>
- Sander, R. (2015). Compilation of Henry's law constants (version 4.0) for water as solvent. *Atmospheric Chemistry and Physics*, 15(8), 4399–4981. <https://doi.org/10.5194/acp-15-4399-2015>
- Sazonova, T. S., Romanovsky, V. E., Walsh, J. E., & Sergueev, D. O. (2004). Permafrost dynamics in the 20th and 21st centuries along the East Siberian transect. *Journal of Geophysical Research (Atmospheres)*, 109, D01108. <https://doi.org/10.1029/2003JD003680>
- Schädel, C., Beem-Miller, J., Aziz Rad, M., Crow, S. E., Hicks Pries, C. E., Ernakovich, J., Hoyt, A. M., Plante, A., Stoner, S., Treat, C. C., & Sierra, C. A. (2020). Decomposability of soil organic matter over time: The Soil Incubation Database (SIDb, version 1.0) and guidance for incubation procedures. *Earth System Science Data*, 12(3), 1511–1524. <https://doi.org/10.5194/essd-12-1511-2020>
- Schädel, C., Schuur, E. A. G., Bracho, R., Elberling, B., Knoblauch, C., Lee, H., Luo, Y., Shaver, G. R., & Turetsky, M. R. (2014). Circumpolar assessment of permafrost C quality and its vulnerability over time using long-term incubation data. *Global Change Biology*, 20(2), 641–652. <https://doi.org/10.1111/gcb.12417>
- Schaefer, K., Zhang, T., Bruhwiler, L., & Barrett, A. P. (2011). Amount and timing of permafrost carbon release in response to climate warming. *Tellus Series B Chemical and Physical Meteorology B*, 63, 165–180. <https://doi.org/10.1111/j.1600-0889.2011.00527.x>
- Schimel, J. P., & Chapin III, F. S. (2006). Microbial Processes in the Alaskan Boreal Forest. In *Microbial Processes in the Alaskan Boreal Forest*. Oxford University Press. <https://doi.org/10.1093/oso/9780195154313.003.0020>
- Schirrmeister, L., Grosse, G., Schwamborn, G., Andreev, A., Meyer, H., Kunitsky, V. V., Kuznetsova, T., Dorozhkina, M. V., Pavlova, E. Y., Bobrov, A., & Oezen, D. (2003). Late Quaternary history of the accumulation plain north of the Chekanovsky Ridge (Lena Delta, Russia)—A multidisciplinary approach. *Polar Geography*, 27(4), 277–319.
- Schirrmeister, L., Siegert, C., Kuznetsova, T., Kuzmina, S., Andreev, A., Kienast, F., Meyer, H., & Bobrov, A. (2002). Paleoenvironmental and paleoclimatic records from permafrost deposits in the Arctic region of Northern Siberia. *Quaternary International*, 89(1), 97–118. [https://doi.org/10.1016/S1040-6182\(01\)00083-0](https://doi.org/10.1016/S1040-6182(01)00083-0)
- Schuur, E. a. G., McGuire, A. D., Schädel, C., Grosse, G., Harden, J. W., Hayes, D. J., Hugelius, G., Koven, C. D., Kuhry, P., Lawrence, D. M., Natali, S. M., Olefeldt, D., Romanovsky, V. E., Schaefer, K., Turetsky, M. R., Treat, C. C., & Vonk, J. E. (2015). Climate change and the permafrost carbon feedback. *Nature*, 520(7546), 171–179. <https://doi.org/10.1038/nature14338>

- Schuur, E. A. G., Vogel, J. G., Crummer, K. G., Lee, H., Sickman, J. O., & Osterkamp, T. E. (2009). The effect of permafrost thaw on old carbon release and net carbon exchange from tundra. *Nature*, 459(7246), 556–559. <https://doi.org/10.1038/nature08031>
- Schwamborn, G., Rachold, V., & Grigoriev, M. N. (2002). Late Quaternary sedimentation history of the Lena Delta. *Quaternary International*, 89(1), 119–134. [https://doi.org/10.1016/S1040-6182\(01\)00084-2](https://doi.org/10.1016/S1040-6182(01)00084-2)
- Serreze, M. C., Walsh, J. E., Chapin, F. S., Osterkamp, T., Dyurgerov, M., Romanovsky, V., Oechel, W. C., Morison, J., Zhang, T., & Barry, R. G. (2000). Observational Evidence of Recent Change in the Northern High-Latitude Environment. *Climatic Change*, 46(1), 159–207. <https://doi.org/10.1023/A:1005504031923>
- Shaver, G.R., Chapin, F., & Gartner, B.L. (1986). Factors limiting seasonal growth and peak biomass accumulation in *Eriophorum vaginatum* in Alaskan tussock tundra. *J Ecol* 74(1):257–278. <https://doi.org/10.2307/2260362>
- Siewert, M. B., Hugelius, G., Heim, B., & Faucherre, S. (2016). Landscape controls and vertical variability of soil organic carbon storage in permafrost-affected soils of the Lena River Delta. *CATENA*, 147, 725–741. <https://doi.org/10.1016/j.catena.2016.07.048>
- Stanley, J.D. (2001). Dating modern deltas: progress, problems, and prognostics. *Annu Rev Earth Planet Sci*, 29(1):257–294. <https://doi.org/10.1146/annurev.earth.29.1.257>
- Tarnocai, C., Canadell, J. G., Schuur, E. a. G., Kuhry, P., Mazhitova, G., & Zimov, S. (2009). Soil organic carbon pools in the northern circumpolar permafrost region. *Global Biogeochemical Cycles*, 23(2). <https://doi.org/10.1029/2008GB003327>
- Treat, C. C., Natali, S. M., Ernakovich, J., Iversen, C. M., Lupascu, M., McGuire, A. D., Norby, R. J., Roy Chowdhury, T., Richter, A., Šantrůčková, H., Schädel, C., Schuur, E. A. G., Sloan, V. L., Turetsky, M. R., & Waldrop, M. P. (2015). A pan-Arctic synthesis of CH₄ and CO₂ production from anoxic soil incubations. *Global Change Biology*, 21(7), 2787–2803. <https://doi.org/10.1111/gcb.12875>
- Treat, C. C., Wollheim, W. M., Varner, R. K., Grandy, A. S., Talbot, J., & Frolking, S. (2014). Temperature and peat type control CO₂ and CH₄ production in Alaskan permafrost peats. *Global Change Biology*, 20(8), 2674–2686. <https://doi.org/10.1111/gcb.12572>
- Trenberth, K. E., Jones, P. D., Ambenje, P., Bojariu, R., Easterling, D., Tank, A. K., Parker, D., Renwick, J. A., Adler, R., Alexander, L., Alexandersson, H., Allan, R., Baldwin, M. P., Beniston, M., Bromwich, D., Camilloni, I., Cassou, C., Cayan, D. R., Chang, E. K. M., ... Jallow, B. (o. J.). *Observations: Surface and Atmospheric Climate Change*. 102.
- Valentine, D. W., Holland, E. A., & Schimel, D. S. (1994). Ecosystem and physiological controls over methane production in northern wetlands. *Journal of Geophysical Research*, 99(D1), 1563. <https://doi.org/10.1029/93JD00391>
- van Huissteden, J., Maximov, T. C., & Dolman, A. J. (2005). High methane flux from an arctic floodplain (Indigirka lowlands, eastern Siberia). *Journal of Geophysical Research: Biogeosciences*, 110(G2). <https://doi.org/10.1029/2005JG000010>
- Veremeeva, A., Glushkova, N., Günther F., Nitze I., & Grosse, G. (2016). Landscapes and thermokarst lake area changes in Yedoma regions under modern climate conditions, Kolyma lowland tundra. XI. International Conference on Permafrost, Potsdam, Germany, 2016-06-20-2016-06-24. <https://doi.org/10.2312/GFZ.LIS.2016.001>
- Wagner, D., Gattinger, A., Embacher, A., Pfeiffer, E.-M., Schloter, M., & Lipski, A. (2007). Methanogenic activity and biomass in Holocene permafrost deposits of the Lena Delta, Siberian Arctic and its implication for the global methane budget.

- Global Change Biology*, 13(5), 1089–1099. <https://doi.org/10.1111/j.1365-2486.2007.01331.x>
- Waldrop, M. P., Wickland, K. P., White, R., Berhe, A. A., Harden, J. W., & Romanovsky, V. E. (2010). Molecular investigations into a globally important carbon pool: Permafrost-protected carbon in Alaskan soils. *Global Change Biology*, 16(9), 2543–2554.
- Walker, H. J. (1998). Arctic Deltas. *Journal of Coastal Research*, 14(3), Article 3. <https://journals.flvc.org/jcr/article/view/80664>
- Walz, J., Knoblauch, C., Tigges, R., Opel, T., Schirrmeister, L., & Pfeiffer, E.-M. (2018). Greenhouse gas production in degrading ice-rich permafrost deposits in northeastern Siberia. *Biogeosciences*, 15(17), 5423–5436. <https://doi.org/10.5194/bg-15-5423-2018>
- Weintraub, M. N., & Schimel, J. P. (2003). Interactions between Carbon and Nitrogen Mineralization and Soil Organic Matter Chemistry in Arctic Tundra Soils. *Ecosystems*, 6(2), 129–143.
- Wetterich, S., Kuzmina, S., Andreev, A. A., Kienast, F., Meyer, H., Schirrmeister, L., Kuznetsova, T., & Sierralta, M. (2008). Palaeoenvironmental dynamics inferred from late Quaternary permafrost deposits on Kurungnakh Island, Lena Delta, Northeast Siberia, Russia. *Quaternary Science Reviews*, 27(15–16), 1523–1540. <https://doi.org/10.1016/j.quascirev.2008.04.007>
- Windirsch, T., Grosse, G., Ulrich, M., Schirrmeister, L., Fedorov, A. N., Konstantinov, P. Y., Fuchs, M., Jongejans, L. L., Wolter, J., Opel, T., & Strauss, J. (2020). Organic carbon characteristics in ice-rich permafrost in alas and Yedoma deposits, central Yakutia, Siberia. *Biogeosciences*, 17(14), 3797–3814. <https://doi.org/10.5194/bg-17-3797-2020>
- Yershov, E. D., Kondrat'yeva, K. A., Loginov, V. F., & Sychev, I. K. (1991). Geocryological Map of Russia and Neighbouring Republics, Faculty of Geology, Chair of Geocryology, Lomonosov Moscow State University.
- Zhang, T., Barry, R. G., Knowles, K., Heginbottom, J. A., & Brown, J. (1999). Statistics and characteristics of permafrost and ground-ice distribution in the Northern Hemisphere. *Polar Geography*, 23(2), 132–154. <https://doi.org/10.1080/10889379909377670>
- Zimov, S. A., Schuur, E. A. G., & Chapin, F. S. (2006). Permafrost and the Global Carbon Budget. *Science*, 312(5780), 1612–1613. <https://doi.org/10.1126/science.1128908>
- Zubrzycki, S., Kutzbach, L., Grosse, G., Desyatkin, A., & Pfeiffer, E.-M. (2013). Organic carbon and total nitrogen stocks in soils of the Lena River Delta. *Biogeosciences*, 10(6), 3507–3524. <https://doi.org/10.5194/bg-10-3507-2013>

Appendix

Appendix 1 Study sites and soil profiles of the analyzed soil cores KUR-P18, KUR-P19, SAM-P20, SAM-P21, SAM-P22, SAM-P24, and SAM-P25.

Core Name	Photos of Study Site and Soil Profile	
KUR18-P18		
KUR18-P19		
SAM18-P20		
SAM18-P21		

SAM18-P22



SAM18-P24



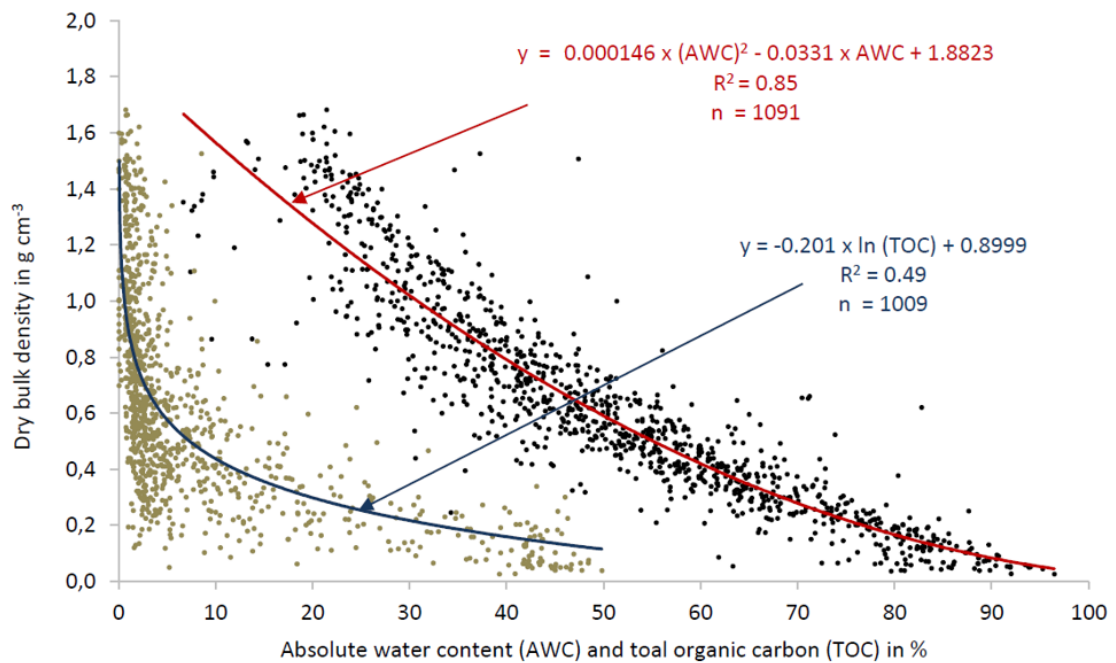
SAM18-P25



Appendix 2 Pore water extraction from thawed soils with Rhizons and syringe, creating a vacuum, which leads to pore water absorption.



Appendix 3 Best-fit correlations between dry bulk density and water content (black dots) or TOC content (brown dots) to estimate dry bulk density (Fuchs, 2019).



Appendix 4 Calculation of added sterilized water to soil samples incubated under anaerobic incubations, when water content of original samples was lower than 30%.

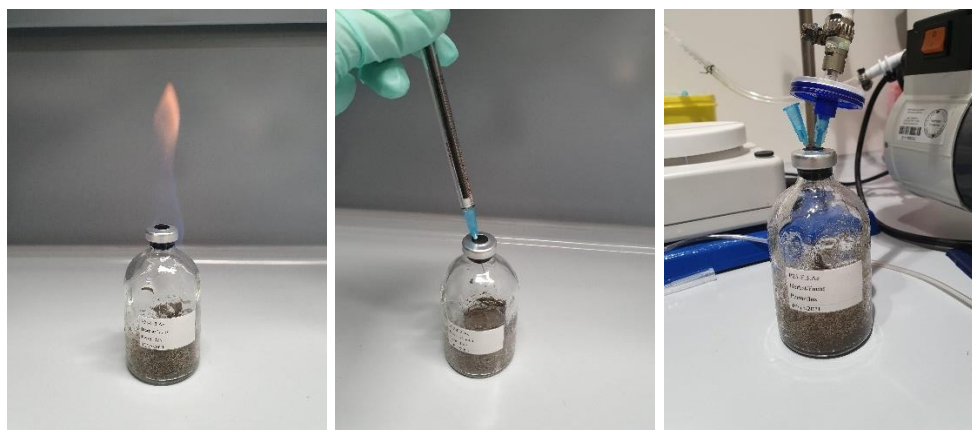
Sample Name	Water Content [-]	Theoretic Wet Weight (g)	Dry Weight [g]	Wet Weight [g]	Added Water [μl]
P19 - active layer	0.17	15.00	12.48	17.83	2829
P19 - permafrost layer	0.35	15.00	9.83	14.04	-
P24 - active layer	0.47	15.00	7.95	11.36	-
P24 - permafrost layer	0.34	15.00	9.86	14.08	-
P25 - active layer	0.17	15.00	12.50	17.85	2850
P25 - permafrost layer	0.17	15.00	12.44	17.76	2764
Blank air	0.00	15.00	15.00	21.43	-
Blank air, sterilized water	0.00	15.00	15.00	21.43	6429

dry weight: weight of dry soil according to the water content of the sample; wet weight: supposed wet weight for a minimum water content θ_w of 30%; added water: difference between wet weight and theoretic wet weight (when the difference was negative, no water was added).

$$\text{dry weight} = \text{theoretic wet weight} \cdot (1 - \text{water content})$$

$$\text{wet weight} = \frac{\text{dry weight}}{1 - \theta_w}$$

Appendix 5 Inflaming of rubber stoppers with 99% ethanol, sampling of 350 μL headspace gas with a Hamilton gastight syringe, and flushing of headspace gas



Appendix 6 Soil characteristics for all analyzed 48 samples as well as six samples from Landgraf (2020).

Sample	layer	Sample depth [cm]	pH [-]	conductivity [$\mu\text{S cm}^{-1}$]	water content [wt%]	dry bulk density [g cm^{-3}]	TOC [wt%]	TN [wt%]	C/N [-]
KUR18-P18-1	Active	1-8	7.57	151	12	1.5	0.29	< 0.10	-
KUR18-P18-2	Active	17-24	7.19	138	21	1.25	1.09	< 0.10	-
KUR18-P18-3	Active	31-38	7.15	224	25	1.16	0.69	< 0.10	-
KUR18-P18-4	Active	46-53	7.27	238	20	1.28	0.26	< 0.10	-
KUR18-P18-5	Active	62-69	7.73	376	22	1.22	0.13	< 0.10	-
KUR18-P19-1	Active	0-5.5	7.78	OFL	38	0.84	3.24	0.19	16.90
KUR18-P19-2	Active	10-17	7.2	400	31	1.01	1.62	0.11	14.56
KUR18-P19-3	Active	23-30	7.78	299	17	1.37	0.34	< 0.10	-
KUR18-P19-4	Active	40-47	7.72	298	19	1.30	0.68	< 0.10	-
KUR18-P19-5	Active	60-67	7.23	295	31	1.00	1.93	0.13	15.42
KUR18-P19-6	Active	73-80	6.86	222	32	0.96	2.01	0.13	15.32
KUR18-P19-7	Permafrost	82-87	6.89	194	35	0.91	1.56	0.11	14.54
KUR18-P19-8	Permafrost	97-102	6.86	228	40	0.78	1.91	0.13	14.94
KUR18-P19-9	Permafrost	106.5-112	6.96	386	37	0.86	1.04	< 0.10	-
SAMI8-P20-1	Active	0-1.5	-	-	33	0.94	2.39	0.13	18.00
SAMI8-P20-2	Active	12-19	-	-	17	1.37	0.67	< 0.10	-
SAMI8-P20-3	Active	28-35	7.22	167	27	1.1	1.44	0.10	14.37
SAMI8-P20-4	Active	40-47	7.24	131	20	1.28	0.54	< 0.10	-
SAMI8-P20-5	Active	55-62	7.04	205	27	1.09	1.64	0.10	16.23
SAMI8-P20-6	Active	74-81	7.23	253	29	1.05	1.55	0.10	15.30
SAMI8-P20-7	Permafrost	90-94.5	6.88	265	47	0.64	3.27	0.20	16.49
SAMI8-P20-8	Permafrost	102-107	6.93	241	29	1.03	1.21	< 0.10	-
SAMI8-P20-9	Permafrost	110-114.5	6.87	276	44	0.7	2.78	0.17	16.32
SAMI8-P21-1	Active	0-2	-	-	43	0.73	3.69	0.24	15.66
SAMI8-P21-2	Active	3-10	-	-	33	0.95	1.72	0.11	16.07

SAM18-P21-3	Active	10-17	7.47	529	21	1.25	1.04	< 0.10	-
SAM18-P21-4	Active	25-32	7.27	456	38	0.83	3.82	0.20	18.95
SAM18-P21-5	Active	43-50	7.2	338	35	0.91	2.40	0.16	15.49
SAM18-P21-6	Permafrost	60-64.5	7.33	146	21	1.24	0.32	< 0.10	-
SAM18-P21-7	Permafrost	76-81	7.44	126	22	1.23	0.45	< 0.10	-
SAM18-P21-8	Permafrost	88-93	6.96	300	44	0.71	2.85	0.18	15.80
SAM18-P21-9	Permafrost	100-104.5	7.28	349	41	0.77	2.38	0.17	14.47
SAM18-P22-1	Active	3-10	-	-	8	1.64	< 0.10	< 0.10	-
SAM18-P22-2	Active	14-21	-	-	12	1.5	< 0.10	< 0.10	-
SAM18-P22-3	Active	25-32	7.62	162	18	1.34	0.11	< 0.10	-
SAM18-P22-4	Active	35-42	7.56	228	19	1.31	0.19	< 0.10	-
SAM18-P22-5	Active	53-66	7.34	233	21	1.25	0.39	< 0.10	-
SAM18-P24-1	Active	0-5	7.57	914	45	0.69	5.52	0.22	24.75
SAM18-P24-2	Active	8-15	7.26	520	35	0.90	2.93	0.14	21.69
SAM18-P24-3	Active	25-32	7.46	310	47	0.65	4.57	0.22	21.28
SAM18-P24-4	Active	40-47	6.99	205	32	0.96	1.82	< 0.10	-
SAM18-P24-5	Permafrost	55-60	7.42	338	24	1.16	0.59	< 0.10	-
SAM18-P24-6	Permafrost	71-75.5	7.18	279	35	0.89	2.85	0.12	24.33
SAM18-P24-7	Permafrost	75.5-82	7.11	224	34	0.92	1.39	< 0.10	-
SAM18-P24-8	Permafrost	89.5-95	7.73	123	19	1.32	0.18	< 0.10	-
SAM18-P25-1	Active	0-4.5	7.68	1342	41	0.77	7.39	0.39	19.19
SAM18-P25-2	Active	8-15	7.62	384	36	0.87	3.74	0.20	18.43
SAM18-P25-3	Active	16-23	7.53	295	37	0.85	3.87	0.22	17.93
SAM18-P25-4	Active	27-35	7.46	110	17	1.37	0.16	< 0.10	-
SAM18-P25-5	Active	46-53	7.62	212	22	1.24	0.17	< 0.10	-
SAM18-P25-6	Permafrost	59-64	7.58	171	23	1.19	0.62	< 0.10	-
SAM18-P25-7	Permafrost	71-76	7.63	219	31	1.00	2.10	0.10	20.20
SAM18-P25-8	Permafrost	85-90	7.81	199	17	1.36	0.18	< 0.10	-
SAM18-P25-9	Permafrost	98-102	7.21	184	27	1.09	1.16	< 0.10	-

Appendix 7 Grain size fractions in volume percent, textural groups and distribution type.

Sample name	sand [vol%]	silt [vol%]	clay [vol%]	textural group	distribution
KUR18-P18-1	93.5	5.5	1.0	sand	unimodal
KUR18-P18-2	77.7	19.5	2.8	silty sand	unimodal
KUR18-P18-3	91	7.6	1.4	silty sand	Bimodal
KUR18-P18-4	95.1	4	0.8	sand	unimodal
KUR18-P18-5	99.2	0.5	0.3	sand	unimodal
KUR18-P19-1	39.5	54.4	6.1	sandy silt	trimodal
KUR18-P19-2	56.9	38.6	4.5	silty sand	polymodal
KUR18-P19-3	92.7	6.3	1.0	sand	unimodal
KUR18-P19-4	94.5	4.7	0.7	sand	unimodal
KUR18-P19-5	59.3	37	3.7	silty sand	bimodal
KUR18-P19-6	49.7	45	5.2	sandy silt	polymodal
KUR18-P19-7	66.5	29.7	3.8	silty sand	bimodal
KUR18-P19-8	51.8	43.6	4.7	silty sand	bimodal
KUR18-P19-9	72.1	24.9	3	silty sand	trimodal
SAM18-P20-3	70.9	26	3.1	silty sand	bimodal
SAM18-P20-4	93.5	5.6	0.9	sand	unimodal
SAM18-P20-5	81.1	16.9	2	silty sand	bimodal
SAM18-P20-6	79.7	18.1	2.2	silty sand	unimodal
SAM18-P20-7	26.5	65.6	7.9	sandy silt	trimodal
SAM18-P20-8	64.8	31.5	3.6	silty sand	trimodal
SAM18-P20-9	44	50.4	5.6	sandy silt	trimodal
SAM18-P21-3	79.7	18.2	2.1	silty sand	unimodal
SAM18-P21-4	50.7	44.6	4.7	sandy silt	trimodal
SAM18-P21-5	39.3	54.1	6.6	sandy silt	bimodal
SAM18-P21-6	94.5	4.5	1	sand	unimodal
SAM18-P21-7	90.6	8.2	1.1	silty sand	unimodal
SAM18-P21-8	36	58.1	5.9	sandy silt	trimodal
SAM18-P21-9	36.1	57.4	6.6	sandy silt	trimodal
SAM18-P22-3	99.4	0.6	0	sand	unimodal
SAM18-P22-4	99.2	0.5	0.4	sand	unimodal
SAM18-P22-5	78.7	18.7	2.7	silty sand	unimodal
SAM18-P24-1	33.1	60.2	6.7	sandy silt	trimodal
SAM18-P24-2	60.7	35.2	4	silty sand	bimodal
SAM18-P24-3	31.9	60.3	7.8	sandy silt	polymodal
SAM18-P24-4	76	21.1	2.9	silty sand	unimodal
SAM18-P24-5	85.5	12.9	1.6	silty sand	bimodal
SAM18-P24-6	77.4	20.3	2.3	silty sand	bimodal
SAM18-P24-7	67.7	29.5	2.9	silty sand	bimodal
SAM18-P24-8	97.5	2	0.5	sand	unimodal
SAM18-P25-1	24.5	66.9	8.6	sandy silt	polymodal
SAM18-P25-2	55.5	40.4	4.1	silty sand	trimodal
SAM18-P25-3	43.1	50.7	6.2	sandy silt	polymodal
SAM18-P25-4	96.9	2.5	0.6	sand	unimodal
SAM18-P25-5	97.2	2.3	0.5	sand	unimodal
SAM18-P25-6	83.4	14.7	1.8	silty sand	unimodal
SAM18-P25-7	85.1	13.3	1.7	silty sand	unimodal
SAM18-P25-8	96.9	2.5	0.6	sand	unimodal
SAM18-P25-9	82.2	15.7	2.1	silty sand	unimodal

Declaration

Tanja Herbst

Name of Student

I hereby declare that I am the sole author and composer of my thesis and that no other sources or learning aids, other than those listed, have been used. Further-more, I declare that I have acknowledged the work of others by providing detailed references of said work. I also hereby declare that my thesis is or has not been prepared for another examination or assignment, either in its entirety or excerpts thereof.

Willmars, 17.03.2022

Place, Date

Tanja Herbst

Signature